JCI The Journal of Clinical Investigation

Chitinase-3-like-1 protein complexes modulate macrophage-mediated immune suppression in glioblastoma

Apeng Chen, Yinan Jiang, Zhengwei Li, Lingxiang Wu, Ulises Santiago, Han Zou, Chunhui Cai, Vaibhav Sharma, Yongchang Guan, Lauren H. McCarl, Jie Ma, Yijen L. Wu, Joshua Michel, Yi Shi, Liza Konnikova, Nduka M. Amankulor, Pascal O. Zinn, Gary Kohanbash, Sameer Agnihotri, Songjian Lu, Xinghua Lu, Dandan Sun, George K. Gittes, Qianghu Wang, Xiangwei Xiao, Dean Yimlamai, Ian F. Pollack, Carlos J. Camacho, Baoli Hu

J Clin Invest. 2021. https://doi.org/10.1172/JCI147552.

Research In-Press Preview **Oncology**

Graphical abstract

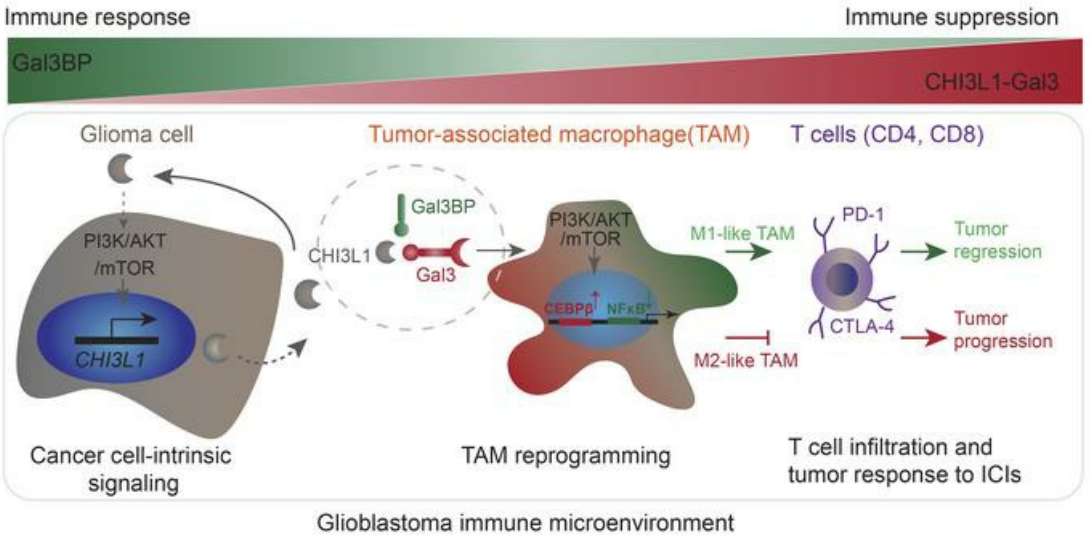

Find the latest version:

https://jci.me/147552/pdf

Chitinase-3-like-1 Protein Complexes Modulate Macrophage-Mediated Immune Suppression in Glioblastoma

Apeng Chen[1,2], Yinan Jiang[2,3], Zhengwei Li[1,2,4], Lingxiang Wu[5], Ulises Santiago[6], Han Zou[1,2], Chunhui Cai[7], Vaibhav Sharma[1,2], Yongchang Guan[1,2,8], Lauren H McCarl[1,2], Jie Ma[2,3], Yijen L Wu[2,9], Joshua Michel[2], Yi Shi[10], Liza Konnikova[11], Nduka M Amankulor[2], Pascal O Zinn[2], Gary Kohanbash[1,2], Sameer Agnihotri[1,2], Songjian Lu[7], Xinghua Lu[7], Dandan Sun[12], George K Gittes[2,3], Qianghu Wang[5], Xiangwei Xiao[2,3], Dean Yimlamai[13], Ian F Pollack[1,2], Carlos J Camacho[5], Baoli Hu[1,2,14*]

[1]Department of Neurological Surgery, [3]Department of Pediatric Surgery, [6]Department of Computational and Systems Biology, [7]Department of Biomedical Informatics, [9]Department of Developmental Biology, [10]Department of Cell Biology, [12]Department of Neurology, University of Pittsburgh School of Medicine, Pittsburgh, PA 15213 USA

[2]John G. Rangos Sr. Research Center, UPMC Children's Hospital of Pittsburgh, Pittsburgh, PA 15214 USA

[4]Department of Neurosurgery, Zhongnan Hospital, Wuhan University, Wuhan, Hubei 430071, China

[5]Department of Bioinformatics, Nanjing Medical University, Nanjing 211166, China

[8]Department of Neurosurgery, The Fourth Hospital of China Medical University, Shenyang, Liaoning, China

[11]Section of Neonatal, Perinatal Medicine, Department of Pediatrics and Obstetrics, Gynecology, and Reproductive Sciences, Yale University School of Medicine, New Haven, CT 06510 USA

[13]Section of Pediatric Gastroenterology and Hepatology, Department of Pediatrics, Yale University School of Medicine, New Haven, CT 06519 USA

[14]Cancer Biology Program, UPMC Hillman Cancer Center, Pittsburgh, PA 15232 USA

***Correspondence:** Baoli Hu, PhD, Department of Neurological Surgery, University of Pittsburgh School of Medicine, Pittsburgh, PA 15213 USA; Tel: 412-692-9457; Email: baolihu@pitt.edu

Conflicts of Interest

B. Hu, C. Camacho, and A. Chen have a provisional patent (NO. 63/159,128) with the University of Pittsburgh. The other authors declare no potential conflicts of interest.

Abstract

Glioblastoma is a highly malignant and incurable brain tumor characterized by intrinsic and adaptive resistance to immunotherapies. However, how glioma cells induce tumor immunosuppression and escape immunosurveillance remains poorly understood. Here, we find upregulation of cancer-intrinsic Chitinase-3-like-1 (CHI3L1) signaling modulating an immunosuppressive microenvironment by reprogramming tumor-associated macrophages (TAMs). Mechanistically, CHI3L1 binding with Galectin-3 (Gal3) selectively promotes TAM migration and infiltration with a protumor M2-like but not an antitumor M1-like phenotype *in vitro* and *in vivo,* governed by a transcriptional program of NFκB/CEBPβ in the CHI3L1/Gal3-PI3K/AKT/mTOR axis. Conversely, Galectin-3-binding protein (Gal3BP) negatively regulates this process by competing with Gal3 to bind CHI3L1. Administration of a Gal3BP mimetic peptide in syngeneic glioblastoma mouse models reverses immune suppression and attenuates tumor progression. These results shed light on the role of CHI3L1 protein complexes in immune evasion by glioblastoma and as a potential immunotherapeutic target for this devastating disease.

Introduction

Glioblastoma (GBM), the most common and lethal primary brain tumor with a median survival rate of only 15 months, remains incurable despite intensive multimodal treatment of surgical resection, radio-chemotherapy, and anti-angiogenic therapy with bevacizumab (1-3). While immunotherapies have been highly effective against some types of cancer, the disappointing results of clinical trials for GBM immunotherapy represent continued challenges (4, 5). Therefore, effective therapies for patients with GBM are urgently needed.

GBM is highly immunosuppressive and resistant to immunotherapy because glioma cells escape effective antitumor immunity by programing the tumor microenvironment (TME) (5, 6). Tumor-associated macrophages/microglia (TAMs), the major component of the GBM TME, account for up to 30%-50% of total tumor composition (7). GBM TAMs originate from bone marrow-derived blood monocytes (monocyte-derived macrophages, MDMs) and brain resident microglia (MG) (7, 8). Previous studies reported that MG account for approximately 15% of TAMs and mainly localize in peritumoral areas, whereas MDMs preferentially localize in intratumoral regions and constitute approximately 85% of the total TAM population. MDMs significantly contribute to the immunosuppressive microenvironment of high-grade glioma (9, 10), suggesting different functions of MG and MDMs within the GBM TME. Increasing evidence indicates that protumor M2-like TAMs are frequently accumulated and associated with higher-grade tumors (11, 12). In contrast, repolarization of TAMs toward an antitumor M1-like phenotype results in tumor regression by producing pro-inflammatory cytokines and key molecules to stimulate T cell antitumor response. This suggests a potential therapeutic strategy of converting M2-like to M1-like TAMs for the treatment of GBM (7, 13). Therefore, the classification of M1/M2-like TAM phenotypes and the functional plasticity of TAMs regulated through glioma cell-intrinsic mechanisms remain an area of active investigation.

Here, we identified that CHI3L1, also known as human homolog YKL-40, predominately modulates the GBM TME using unbiased approaches. CHI3L1 signaling selectively regulates tumor infiltration and cell migration of MDMs and MG by forming distinct protein binding complexes. CHI3L1 protein complexes further reprogram TAMs to regulate T cell-mediated immune response in GBM progression. Importantly, we developed a peptide to disrupt CHI3L1 protein complexes, which can promote tumor regression in a syngeneic mouse GBM model, providing a potential therapeutic strategy to eradicate this devastating brain tumor.

Results

Cancer-cell-intrinsic CHI3L1 is regulated by the PI3K/AKT/mTOR pathway in a positive feedback loop

We previously developed a *de novo* GBM model using a myristoylated form of AKT (myr-AKT) and dominant-negative p53 (p53DN)-engineered human neural stem cells (hNSCs), thereby enabling us to perform precise system-level comparisons between hNSCs and their derived glioblastoma stem cells (GSCs) (14). To identify cancer-cell-intrinsic factors for malignant transformation, we performed global analyses of differentially expressed genes between hNSCs and GSCs. CHI3L1 is the most significantly upregulated gene in GSCs derived from hNSCs overexpressing myr-AKT and p53DN (**Figure 1A**). *In vitro* and *in vivo* validations revealed that CHI3L1 is highly expressed in GSCs and their derived tumors with activated AKT signaling (**Figure 1, B**-**D**). By contrast, inhibiting AKT/mTOR signaling by rapamycin decreased *CHI3L1* mRNA and protein expression in hNSC-p53DN-AKT (**Figure 1, E** and **F**).

CHI3L1 is a secreted glycoprotein with chitin-binding capacity but lacking chitinase activity (15), which plays a role in tissue remodeling, inflammation, and cancer (16). Although CHI3L1 is highly expressed and associated with a poor clinical outcome in GBM patients (17, 18), CHI3L1 regulation and its molecular mechanism(s) of action remain undefined. To test the hypothesis that CHI3L1 is predominantly upregulated by the PI3K/AKT/mTOR signaling pathway, we treated the GBM neurosphere line TS603 and U87 cells with NVP-BEZ235 (a dual PI3K and mTOR inhibitor). Immunoblot analysis revealed that CHI3L1 expression was regulated by PI3K/AKT/mTOR signaling in a time- and dose-dependent manner (**Figure 1, G** and **H,** and **Supplemental Figure 1, A** and **B**). Furthermore, we measured CHI3L1 levels in the conditioned media (CM) of two GBM neurosphere lines treated with NVP-BEZ235 or NVP-BKM120 (a pan-PI3K kinase inhibitor). Inhibition of PI3K/AKT/mTOR activation decreased CHI3L1 secretion in a dose- and time-dependent manner (**Figure 1, I** and **J,** and **Supplemental Figure 1, C** and **D**). Importantly, the CM from GBM neurosphere line TS543 overexpressing CHI3L1 enhanced pAKT, pS6, and CHI3L1 levels over control in TS543 cells (**Figure 1K**). Conversely, overexpression of myr-AKT dramatically increased CHI3L1 levels in TS543 (**Figure 1L**). These results demonstrate a positive feedback loop between CHI3L1 and the PI3K/AKT/mTOR signaling.

We analyzed a previously published single-cell GBM transcriptomic patient dataset (19), finding that glioma cells express high levels of CHI3L1 and may represent a major source of CHI3L1 in the GBM TME (**Supplemental Figure 1, E**-**G**). In The Cancer Genome Atlas (TCGA) GBM datasets, CHI3L1 is highly expressed in tumors

versus non-tumor tissues and mesenchymal versus proneural and classical subtypes (**Figure 1M** and **Supplemental Figure 1H**). Moreover, higher levels of *CHI3L1* mRNA expression are significantly associated with *PTEN* deletions/mutations, PI3K/AKT/mTOR signaling activation, and poor outcome in patients with IDH wildtype (IDHwt) GBM (**Figure 1, N** and **O**, and **Supplemental Figure 1, I** and **J**). Together, these results reinforce that a positive regulatory feedback loop of the PI3K/AKT/mTOR-CHI3L1 signaling may play a pivotal role in regulating GBM progression and treatment response.

CHI3L1 plays a predominant role in shaping the landscape of the GBM immune TME

To determine the main function of CHI3L1 in GBM, we performed *in vivo* CHI3L1 gain-of-function studies in an orthotopic xenograft model of TS543 intracranially implanted in severe combined immunodeficiency (SCID) mice. Surprisingly, enforced CHI3L1 expression did not significantly promote tumor progression compared with vector controls (**Supplemental Figure 2, A-C**). From the GBM TCGA dataset, CHI3L1 correlated genes (1,960 genes) are mainly associated with cellular movement, immune cell trafficking, and cell-to-cell signaling by Ingenuity Pathway Analysis (IPA) (**Figure 2A** and **Supplemental Table 1**). These data indicate that CHI3L1 may play a pivotal role in regulating the GBM immune TME. To this end, we compared tumor progression between SCID and immunocompetent (C57BL/6) mice intracranially implanted with murine glioma GL261 cells that have low levels of endogenous CHI3L1 but forced expression of human *CHI3L1* gene (GL261-CHI3L1) (**Figure 2, B** and **C**). Notably, CHI3L1 overexpression increased tumor size and decreased survival in C57BL/6 mice, but not in SCID mice (**Figure 2, D** and **E**). Conversely, we generated an orthotopic syngeneic mouse model of GBM using QPP7 cells that were derived from a spontaneous murine glioma model *Nes-CreER*^{T2}*Qk*$^{L/L}$*Pten*$^{L/L}$*Trp53*$^{L/L}$ (20) with high levels of endogenous CHI3L1 (**Figure 2F and Supplemental Figure 2D**). *In vivo* loss-of-function studies revealed that knockdown (KD) of the mouse *Chi3l1* gene (shChi3l1#1 and #2) in QPP7 cells significantly repressed tumor growth in the syngeneic mice by magnetic resonance imaging (MRI) 4 weeks after implantation (**Figure 2F, Supplemental Figure 2, E** and **F**). Importantly, comparative analyses of tumor progression in SCID and C57BL/6 mice bearing QPP7 tumors demonstrated that *Chi3l1* KD decreased tumor size and extended the survival of immunocompetent mice, but not immunodeficient mice (**Figure 2, G** and **H**). Together, these results suggest that CHI3L1 predominantly regulates the tumor immune TME, rather than tumor cells *per se*.

To determine the effect of CHI3L1 on immune cell distribution in the TME of GBM, we analyzed the major cell populations, including TAMs, T cells, Natural Killer (NK) cells, and myeloid-derived suppressor cells (MDSCs). Flow cytometry of tumors revealed that enforced CHI3L1 expression in GL261 mouse models significantly increased the M2-like TAMs ($CD45^+CD11b^+CD14^+MHCII^+Ly6C^-$) but decreased $CD3^+$, $CD4^+$, and $CD8^+$ T cell populations (**Figure 2 I** and **Supplemental Figure 2, G** and **H**). By contrast, *Chi3l1* KD in QPP7 syngeneic models significantly decreased the M2-like TAMs but increased $CD3^+$ and $CD4^+$ T cell populations (**Figure 2J** and **Supplemental Figure 2I**). These findings were further validated by performing single-cell mass cytometry (CyTOF) analysis in the QPP7 tumors with *Chi3l1* KD *vs* controls using the additional markers to identify cell populations (*e.g.*, Arg1, iNOS, F4/80, CD90.2, *etc.*) (**Supplemental Figure 2J**-**L**). Notably, QPP7 tumors, compared to GL216 tumors, did not show significant changes of $CD8^+$ T cells, which may support the low mutational load in QPP7 but not in GL261 cells determining the modest $CD8^+$ T cell infiltration in these syngeneic GBM mouse models (20, 21). Collectively, the gain/loss-of-function studies reveal a predominant role of CHI3L1 in regulating GBM progression by reprogramming the tumor immune microenvironment.

CHI3L1 selectively promotes infiltration of M2-like versus M1-like MDMs and MG

Previous studies reported the involvement of CHI3L1 in macrophage differentiation and recruitment associated with other pathological conditions (22, 23) although the mechanism of its action remains elusive. Furthermore, the M2-like TAMs consistently and significantly changed in response to CHI3L1 expression in our syngeneic mouse models. Therefore, we focused on how CHI3L1 reprograms TAMs in the GBM TME. Further flow cytometry analyses showed that overexpression of CHI3L1 increased the percentage of M2-like TAMs but decreased M1-like TAMs ($CD45^+CD11b^+CD14^+Ly6C^+$) and the M1-/M2-like TAM ratio in GL261 tumor models (**Figure 3A** and **B**). Conversely, *Chi3l1* KD decreased the percentage of M2-like TAMs but increased M1-like TAMs and the M1-/M2-like TAM ratio in QPP7-derived GBM models by flow cytometry (**Figure 3, C** and **D,** and **Supplemental Figure 3, A** and **B**). Moreover, additional markers used for TAM polarization analyses revealed a significant decrease of the $CD45^+CD68^+CD11b^+CD206^+$ and $CD45^+Arg1^+$ populations but an increase in the ratios of $CD206^-/CD206^+$ and $iNOS^+/Arg1^+$ cells in QPP7 tumors (**Figure 3E** and **Supplemental Figure 3C**). These results suggest that CHI3L1 regulates TAM polarization toward M2-like phenotype in the GBM TME.

To specifically investigate CHI3L1-regulated MDMs and MG tumoral infiltration, we performed co-immunofluorescence (IF) staining to detect F4/80, a mature phagocytic cell marker, and P2Y12, a classic marker

for microglia (24, 25). Notably, overexpression of CHI3L1 in GL261-derived glioma models greatly increased F4/80$^+$ cell accumulation in intratumoral regions but did not significantly change infiltration of P2Y12$^+$ MG, which predominantly reside in peritumoral regions (**Figure 3**, **F** and **G**). In contrast, there was a decreased F4/80$^+$ cell infiltration in QPP7-derived gliomas without a significant change of peritumoral P2Y12$^+$ MG in *Chi3l1* KD versus controls (**Figure 3, H** and **I**). Furthermore, intratumoral MDMs (M2-like) were significantly accumulated in GL216-CHI3L1 tumors but reduced in *Chi3l1* KD QPP7 tumors, respectively, based on IF staining using additional markers (CD206 and CD49D) (**Supplemental Figure 3D**-**G**). These data reveal that cancer-cell-intrinsic CHI3L1 promotes accumulation of MDMs over MG within the tumor, which provides a mechanistic explanation for the observation of abundant MDM infiltration in tumor lesions while the preferential occupation of MG in the periphery (9, 10, 19).

To further verify the effect of CHI3L1 on TAM infiltration, we performed *in vitro* scratch-wound healing and transwell assays to examine cell migration of bone marrow-derived macrophages (BMDMs) and microglial cells treated with recombinant CHI3L1 protein (rCHI3L1). We generated and confirmed the polarization states of M0, M1, and M2 macrophages using isolated BMDMs from C57BL/6 mice according to a previous standard protocol (26) (**Supplemental Figure 3H**). Strikingly, rCHI3L1 treatment promoted M2 BMDM migration but not M0 and M1 BMDMs (**Figure 4**, **A** and **B**). However, rCHI3L1 treatment did not increase cell migration in a mouse microglial cell line (SIM-A9) (**Supplemental Figure 3I**), supporting our observation that MG tumor infiltration is unaffected by CHI3L1. Moreover, a transwell assay confirmed that rCHI3L1 promoted cell migration in M2 BMDMs, but not in M0 BMDMs, M1 BMDMs, or microglial cells (**Figure 4C** and **Supplemental Figure 3J**-**M**).

Based on CIBERSORT for gene signatures and correlation analysis in the GBM TCGA datasets (12, 27), *CHI3L1* mRNA expression is positively correlated with tumor-promoting M2-like macrophages but negatively correlated with tumor-killing M1-like macrophages (**Figure 4D**). Furthermore, analysis of gene set signatures (28) revealed that MDMs, rather than MG, are significantly enriched in tumors with higher levels of CHI3L1 expression in GBM patients (**Supplemental Figure 3N**). Altogether, these results demonstrate that CHI3L1 regulates TAM polarization and selectively promotes the migration and accumulation of M2-like MDMs in GBM.

Gal3BP binding to CHI3L1 negatively regulates M2-like macrophage migration

To elucidate how CHI3L1 promotes M2-like MDM migration, we explored CHI3L1 binding proteins using immunoprecipitation coupled to liquid chromatography-mass spectrometry (LC-MS). LC-MS analysis of

extracellular or membrane-associated proteins revealed 7 putative binding proteins encoded by the *ANXA1*, *LGALS3BP*, *GAPDH*, *PDIA6*, *BCAP31*, *ARL6IP5*, and *MARCKS* gene, which are highly associated with CHI3L1 in GBM (**Supplemental Figure 4A**; **Supplemental Table 2**). None of these genes have been previously identified as binding partners of CHI3L1. An orthogonal structure-based screening identified Gal3BP, encoded by the *LGALS3BP* gene, as a possible binding partner of CHI3L1 (**Figure 5**, **A** and **B**). Gal3BP, also known as 90K or Mac-2-binding protein, is a secreted glycoprotein upregulated and involved in innate immunity against viral and bacterial infections (29). Interestingly, the domain of Gal3BP predicted to interact with CHI3L1 corresponds to Gal3BP main dimerization domain (**Supplemental Figure 4B**), indicating that CHI3L1 can bind monomeric Gal3BP to disrupt its dimerization. Co-IF staining demonstrated strong colocalization of Gal3BP and CHI3L1, which was further supported in live cells by co-immunoprecipitation (Co-IP) (**Figure 5**, **C** and **D**).

To test whether Gal3BP binding to CHI3L1 promotes MDM migration, we treated M2 BMDMs with rCHI3L1 and recombinant Gal3BP protein (rGal3BP). Surprisingly, rGal3BP significantly attenuated rCHI3L1-induced M2 BMDM migration, as found by scratch-wound healing assay (**Figure 5E**) and transwell migration assay (**Figure 5F**). Analyzing IF staining of tumors derived from GL261-CHI3L1 bearing syngeneic mice, we observed the mutually exclusive expression patterns of Gal3BP and F4/80 (**Supplemental Figure 4C**), indicating a negative correlation between Gal3BP expression levels and MDM distribution in glioma. Assessment of correlation between Gal3BP expression and gene signatures of M1/M2-like macrophages revealed a significant positive correlation between *LGALS3BP* mRNA expression and M1-like macrophages compared with M2-like macrophages in the GBM TCGA database (**Supplemental Figure 4D**). Furthermore, M1-like macrophage signature was found to be highly enriched in GBMs with low levels of *CHI3L1* expression but high levels of *LGALS3BP* expression, whereas a decrease of M2-like macrophage signature was shown in these tumors (**Figure 5G**). These results indicate that Gal3BP binding to CHI3L1 could negatively regulate CHI3L1-induced M2-like MDM infiltration in the GBM TME.

CHI3L1 binds to Gal3 resulting in selective migration of MDMs, which is negatively regulated by Gal3BP

Gal3, encoded by the *LGALS3* gene as a binding partner of Gal3BP, plays a critical role in macrophage migration and activation (30-32). Therefore, we hypothesized that Gal3 is also involved in CHI3L1-mediated MDM migration. *In silico* docking of the N-terminal domain of Gal3 and CHI3L1 suggests that Gal3 interacts with

CHI3L1 in the same binding pocket as Gal3BP (**Figure 6, A** and **B**). Consistent with this prediction, we verified Gal3-Gal3BP binding as well as Gal3-CHI3L1 binding by Co-IF and Co-IP assays (**Figure 6, C** and **D**). Gal3BP was shown to bind with a conserved carbohydrate recognition domain (CRD) at the C-terminal domain of Gal3 (32). Interestingly, the Co-IP assay demonstrated that TD139, a high-affinity and potent inhibitor of Gal3, completely disrupted Gal3-Gal3BP but not Gal3-CHI3L1 interactions, indicating a novel binding mechanism of Gal3 and CHI3L1(**Figure 6D**). Importantly, Gal3 and Gal3BP are predicting to compete for the same binding site in CHI3L1, which was validated by a Co-IP assay by adding an increasing amount of rGal3BP into the mixture of rCHI3L1 plus recombinant Gal3 protein (rGal3) with or without TD139 treatment *in vitro* (**Figure 6E**). Computational estimates of the interaction free energy between these proteins using the FastContact server (33) suggests that Gal3BP binds to CHI3L1 more strongly than Gal3 ($\Delta G_{binding}$ = -9.9 kcal/mol and -4.3 kcal/mol, respectively). Of note, sequence alignments of the binding domains in CHI3L1, Gal3, and Gal3BP showed high conservation between the human and mouse, indicating the evolutionarily conserved functions of these genes (**Supplemental Figure 5A**).

To examine whether Gal3 and Gal3BP are associated with selective migration of M1/M2-like MDMs, we detected expression levels of Gal3 and Gal3BP in polarized BMDMs. qRT-PCR and immunoblot analyses revealed highly expressed Gal3 in M2 BMDMs compared to M0 and M1 BMDMs (**Supplemental Figure 5, B** and **C**). Interestingly, we observed that a microglia cell line (SIM-A9) expresses higher levels of Gal3BP compared with polarized BMDMs and the murine macrophage cell line RAW264.7 (**Supplemental Figure 5, C** and **D**), indicating a potential mechanism by which CHI3L1 effectively induces cell migration in M2-like MDMs but not MG. We, therefore, hypothesized that CHI3L1 cooperates with Gal3 to selectively promote M2 BMDM migration. To this end, scratch-wound healing and transwell assays revealed that treatment of M0 BMDMs (lower endogenous levels of Gal3 expression) with rCHI3L1+ rGal3 significantly increased cell migration (**Figure 7A**-**D**). To test whether Gal3BP inhibits CHI3L1-Gal3 induced MDM migration, M0 BMDMs were treated with rCHI3L1 + rGal3 + rGal3BP, resulting in a significant decrease in cell migration compared with those treated with rCHI3L1+rGal3 (**Figure 7A**-**D**). These data suggest that Gal3BP competes with Gal3 to bind CHI3L1, leading to inhibition of MDM migration by disrupting the CHI3L1-Gal3 protein complex. We analyzed the enrichment of M1/M2-like macrophage signatures associated with the expression of these genes in TCGA GBM samples and observed increased M2- and decreased M1-like macrophage signatures in tumors with high mRNA expression

levels of *CHI3L1* and *LGALS3* (**Figure 7E**). Furthermore, a significant increase of M1-like macrophage signatures was shown in the GBMs with low levels of *CHI3L1* and *LGALS3* expression but high levels of *LGALS3BP* expression (**Supplemental Figure 5E**), indicating a predominant association between Gal3BP and a proinflammatory M1-like phenotype. Collectively, these results suggest that CHI3L1 binds with Gal3 forming a protein complex, promoting infiltration of M2-like MDMs, which is negatively regulated by Gal3BP via a competitive interaction.

CHI3L1-Gal3 protein complex induces tumor immunosuppression by reprogramming MDMs

To delineate molecular mechanisms of CHI3L1 protein complexes-induced tumor progression, we performed RNA-seq analysis on TAMs isolated from orthotopic xenograft glioma models in C57BL/6 mice bearing the isogenic line QPP7 with shChi3l1, relative to QPP7 with shSC. Gene-Ontology (GO) analysis showed that signaling pathways regulating cell killing, leukocyte-mediated cytotoxicity, and lymphocyte-mediated immunity were enriched in TAMs derived from *Chi3l1* KD tumors (**Figure 8A**). We hypothesized that CHI3L1 signaling reprograms TAMs toward a protumor phenotype, leading to dysregulation of the tumor-infiltrating lymphocyte (TIL)-mediated antitumor immune responses. To this end, we observed that CHI3L1 overexpression significantly decreased the active $CD4^+$ ($CD69^+CD62L^-$) and $CD8^+$ ($CD69^+CD62L^-$) TILs in GL261 tumors (**Figure 8B**). Conversely, the active $CD4^+$ T cells were significantly increased in QPP7 *Chi3l1* KD tumors while enrichment of active $CD8^+$ T cells did not reach significance (**Figure 8C**). These results suggest that dysregulation of T cell-mediated antitumor immune response contributes to CHI3L1-induced tumor progression.

Previous studies revealed that TAM depolarization, rather than depletion, profoundly affects cancer progression by changing gene expression and switching between phenotypes of immune suppression and immune stimulation (34, 35). We further demonstrated that depleting peripheral and intratumoral MDMs but not MG by systemic delivery of clodronate liposomes (36, 37) did not repress tumor progression in the syngeneic orthotopic glioma model of C57BL/6 mice bearing GL261-CHI3L1 (**Supplemental Figure 6, A-E**). Gene set enrichment analysis (GSEA) showed that hallmark pathways in immune stimulation, including IFNα, IFNγ, IL6-JAK-STAT3 signaling, and inflammatory response, were enriched in TAMs derived from tumors with *Chi3l1* KD compared to controls (**Supplemental Figure 6, F** and **G**). Moreover, genes associated with immune suppression (*Arg1*, *Ym1*, *Ccl2*, *Il10*) were downregulated in TAMs from shChi3l1 tumors; however, genes associated with immune stimulation (*Nos2*, *Il6*, *Il12b*, *Ifng*) were upregulated in these TAMs (**Supplemental Figure 6H**). To

further examine the involvement of T cells in CHI3L1-mediated tumor progression, we performed antibody depletion studies of $CD4^+$ and $CD8^+$ cells in GL261-CHI3L1 and QPP7-shChi3l1#1 derived syngeneic tumor models, respectively. Treatment with anti-CD4 and anti-CD8 antibodies significantly enhanced CHI3L1 overexpression-induced tumor progression in GL261 models (**Figure 8, D** and **E**) but attenuated *Chi3l1* KD-mediated tumor regression in QPP7 models (**Figure 8, F** and **G; Supplemental Figure 6I**). Together, these results reveal that silencing CHI3L1 reprograms a TAM switch from immune suppression to stimulation, which is required for T cell-mediated antitumor response.

To elucidate the downstream signaling pathways of CHI3L1 protein complex-regulated TAM reprogramming, we treated M0 BMDMs with rCHI3L1+rGal3. Interestingly, genes related to anti-inflammation (*Arg1*, *Ym1*, *Ccl2, Il10*) were increased compared to any single agent treatment by qRT-PCR assessment. Notably, upregulation of these genes by rCHI3L1+rGal3 treatment was significantly inhibited in M0 BMDMs treated with rGal3BP (**Figure 8H**). These data indicate that the CHI3L1-Gal3 protein complex reprograms TAMs toward an M2-like phenotype by regulating gene expression associated with immune suppression, which is negatively regulated by Gal3BP. Given the positive feedback loop of the CHI3L1-PI3K/AKT/mTOR singling (**Figure 1**), we hypothesized that the CHI3L1-Gal3 protein complex activates the PI3K/AKT/mTOR pathway, which significantly controls a macrophage switch between immune stimulation and suppression by regulating NFκB and CEBPβ activation (35). Immunoblot analysis showed that rCHI3L1 + rGal3 treatment increased the levels of p-AKT (T473 and S308), p-S6, and p-mTOR compared to either agent alone (**Figure 8I**), which were inhibited by the addition of rGal3BP in M0 BMDMs (**Figure 8J**). To evaluate the activation of PI3K/AKT/mTOR downstream transcription factors, we found that rCHI3L1 plus rGal3 stimulated C/EBPβ expression and simultaneously inhibited p65–RelA phosphorylation in M0 BMDMs, which were also reversed by treating with rGal3BP (**Figure 8K**). GSEA showed enrichment of mTOR1 signaling in TAMs derived from tumors with shSC, and enrichment of TNFA signaling via NFκB pathway in TAMs derived from tumors with shChi3l1, further supporting the involvement of these transcription factors in MDM reprogramming by CHI3L1 protein complexes (**Figure 8L**). Collectively, these results indicate that CHI3L1 protein complexes reprogram MDMs toward an immunosuppression or immunostimulation phenotype by controlling a transcriptional regulatory program of PI3K/AKT/mTOR-NFκB/CEBPβ (**Supplemental Figure 6J**).

Gal3BP mimetic peptide inhibits CHI3L1-Gal3 complex-induced tumor progression

To investigate whether disruption of CHI31L-Gal3 protein binding complex can reverse MDM-mediated immune suppression and thereby attenuate glioma progression, we designed a Gal3BP Mimetic Peptide (GMP) to disrupt the interaction between Gal3 and CHI3L1. Molecular dynamics showed that GMP (T_{132}LDLSRELSEALGQI_{146}), rather than scrambled control peptide (SCP, L_1RTRLEETLSSDTSH_{15}), behaves as a linear peptide capable of recapitulating interaction with CHI3L1 (**Figure 9A**). To test GMP inhibiting CHI3L1-Gal3-induced macrophage migration *in vitro*, M2 BMDMs were treated with rCHI3L1 in combination with GMP and SCP, respectively. Of note, scratch-wound healing assay analysis revealed that rCHI3L1-promoted M2 BMDM migration was significantly inhibited by GMP compared with SCP treatment (**Figure 9, B** and **C**). In contrast to SCP, GMP also attenuated rCHI3L1+ rGal3-induced M0 BMDM migration (**Supplemental Figure 7, A** and **B**). To verify that GMP recapitulates Gal3BP to compete with Gal3 binding with CHI3L1, we found that GMP treatment resulted in decreasing binding of CHI3L1 and Gal3 in THP-1 cells by the Co-IP assay (**Figure 9D**). Moreover, GMP inhibits rCHI3L1-induced BMDM migration in a dose-dependent manner (**Supplemental Figure 7C**). These data demonstrate that this new-developed peptide can mimic Gal3BP to disrupt CHI31L-Gal3 protein interaction and BMDM migration.

To assess the antitumor effect of GMP *in vivo*, GMP and SCP were administered directly into brain tumors by an implantable guide-screw system in C57BL/6 mice bearing GL261-CHI3L1 orthotopic tumors. Notably, GMP treatment reduced tumor growth and extended animal survival (median survival of 36 days) compared to SCP (median survival of 29 days) (**Figure 9, E** and **F**). To validate the antitumor effect of GMP on tumors with the endogenous level of CHI3L1, the orthotopic syngeneic mice bearing QPP7 glioma were treated by local delivery of GMP and SCP into the brain, respectively. Consistently, we found that the treatment of GMP decreased tumor size and increased mouse survival in the QPP7 model (**Supplemental Figure 7**, **D** and **E**).

To evaluate the changes of immune cell populations following peptide treatment, we performed flow cytometry of cells harvested from syngeneic C57BL/6 mice bearing GL261-CHI3L1 glioma. Following GMP treatment, an increase of M1-like TAMs (49.5 ± 4.0 % *vs* 38.2 ± 6.7 %, $P = 0.0719$) and decrease of M2-like TAMs (42.8 ± 3.8 % *vs* 52.7 ± 3.9 %, $P = 0.0536$) were observed compared to SCP treatment (**Figure 9G**). In contrast to SCP, GMP treatment significantly increased T cells ($CD3^+$), particularly $CD8^+$ cells (**Figure 9H** and **Supplemental Figure 7F**). The $CD4^+$ cell population increased under GMP versus SCP treatment (41.9 ± 4.5 % *vs* 39.8± 4.0 %), indicating that Tregs, a subset of $CD4^+$ cells, could influence the total CD4 cell composition,

proliferation, and recruitment (**Supplemental Figure 7G)**. These results suggest that GMP could reprogram TAMs from protumor to antitumor phenotype, which indirectly promotes $CD8^+$ T cell-mediated antitumor immune response.

Despite increasing the tumor-infiltrating T cells after GMP treatment, T cell exhaustion is a hallmark of GBM local immune dysfunction due to the upregulation of multiple immune checkpoints such as PD-1 and CTLA-4 (38, 39). Therefore, we assessed expression levels of these immune checkpoints in $CD4^+$ and $CD8^+$ T cells; and found that both PD-1 and CTLA-4 were significantly upregulated in $CD8^+$ T cells from GMP-treated tumors compared to those in the SCP-treated tumors in the GL216-CHI3L1 model (**Figure 9H**). The $CD4^+$ T cells from tumor-bearing mice displayed a trend of elevated levels of PD-1 and CTLA-4 following the treatment with GMP *vs* SCP, respectively (**Supplemental Figure 7G**). We also evaluated the expression of PD-L1, a ligand of PD-1, which is upregulated in activated leukocytes and cancer cells (40). Interestingly, GMP treatment significantly decreased PD-L1 expression in $CD45^+$, $CD8^+$, and glioma cells, which suggests that disrupting CHI3L1-Gal3 interaction may lead to the reduction of T cell exhaustion (**Supplemental Figure 7, H** and **I**).

Together, our results indicate that CHI3L1 protein binding complexes with Gal3 or Gal3BP modulate TAM-mediated immune suppression and stimulation, leading to resistance or response to immune checkpoint therapy. To evaluate whether gene expression of *CHI3L1*, *LGALS3,* and *LGALS3BP* is associated with patient response to immunotherapy with immune checkpoint inhibitors (ICIs), we analyzed bulk RNA-sequencing profiles of GBM from 16 GBM patients with treatment of PD-1 inhibitors (nivolumab or pembrolizumab) (41). Consistently, higher levels of *LGALS3BP* expression are associated with anti-PD-1 responders, whereas lower levels of *LGALS3BP* expression are associated with anti-PD-1 non-responders (**Figure 10A** and **Supplemental Figure 7J**). Moreover, higher levels of *LGALS3BP* combined with lower levels of *LGALS3* and/or lower levels of *CHI3L1* are associated with anti-PD-1 responders and *vice versa* (**Figure 10A**). Collectively, these data suggest that the CHI3L1 protein binding complex modulates TAM and T cell-mediated immunity, which underlies these proteins as the key determinants of the response to immune checkpoint therapy. Therapeutically, disrupting the CHI3L1-Gal3 protein complex using GMP may synergize with ICIs to effectively promote tumor regression for GBM patients (**Figure 10B**).

Discussion

Although the GBM TME plays a crucial role in regulating tumor progression and is increasingly recognized as a therapeutic target, understanding the underlying cellular and molecular mechanisms governing glioma cells and their surrounding components remains challenging. In this study, we discovered that cancer-cell-intrinsic CHI3L1 plays a predominant role in modulating the GBM TME by forming a protein complex with Gal3 or Gal3BP to promote macrophage-mediated immune suppression. Our efforts to understand the mechanisms governing GBM immune suppression resulted in a newly developed peptide as an immunostimulatory drug candidate and pharmacological modifications of CHI3L1-Gal3/Gal3BP protein complexes as potential therapeutics for patients with GBM.

Increasing evidence suggests that tumor-intrinsic mechanisms dictate various non-cancerous cells within the tumor microenvironment, which exert multifaceted functions, ranging from antitumor to protumor activities (12, 13, 42). The findings in this study demonstrate that cancer-cell intrinsic CHI3L1 is upregulated by the PI3K/AKT/mTOR signaling axis in a positive feedback loop, which plays a predominant role in modulating the GBM immune microenvironment by inducing M2-like MDM infiltration and repolarization in a paracrine mechanism. Genetically, *CHI3L1* gene expression is significantly associated with loss of chromosome 10q encompassing *PTEN* in GBM (18). Our work reinforces the positive correlation between *CHI3L1* gene expression and *PTEN* deletions/mutations or other mechanisms leading to PI3K/AKT/mTOR activation (*e.g.* NF1 mutations). These findings deepen our understanding of tumor-intrinsic signaling pathways driven by genetic alterations in the regulation of the GBM immune microenvironment for tumor progression and treatment response.

In exploring the role of CHI3L1 for regulating the GBM immune microenvironment, we discovered that CHI3L1 binding with Gal3 promotes MDM infiltration and reprograms MDMs toward a tumor-promoting M2-like phenotype, which is negatively regulated by Gal3BP. Increased expression and secretion of Gal3 were observed in both human and mouse M2-polarized macrophages compared to monocytes and M1-polarized macrophages (30, 43). However, increased levels of Gal3BP and a proinflammatory phenotype were observed in human monocyte-derived M1 macrophages *in vitro* and plasma from patients with cardiovascular disease or hepatitis C infection (44, 45). In this study, our finding of CHI3L1-Gal3 protein complex-induced selective migration of M2-polarized BMDMs provides a mechanistic explanation for a long-standing observation, namely highly infiltrating M2-like MDMs associated with both human and mouse GBM (9, 10, 12, 19). In addition to promoting M2-like

MDM accumulation, the present study also provides the mechanisms for immunosuppression that enables GBM to escape immune surveillance, by which CHI3L1-Gal3 protein complex activates AKT/mTOR-mediated transcriptional regulatory network (NFκB and CEBPβ), leading to a macrophage switch toward immune suppression from immune stimulation (35).

Reducing immunosuppression and overcoming immunotherapy resistance are becoming therapeutic areas of great interest for the treatment of GBM as well as other solid tumors (46, 47). Our findings provide a rationale for disrupting the CHI3L1-Gal3 protein complex by the addition of Gal3BP to reduce the degree of tumor immunosuppression and improve antitumor immune response in the GBM TME. Interestingly, a previous study showed that local and systemic increases in Gal3BP levels inhibited tumor growth by stimulation of the residual cell-mediated immune defense of the nude mouse (48). Although the function of Gal3BP is controversial in physiologic and pathologic conditions, elevated levels of Gal3BP in bacterial and viral infections and the neoplastic context suggest its crucial role in immune response as an immunostimulatory molecule (29, 49, 50). In our study, GMP being locally delivered into brain tumor led to tumor regression in the treated animals combined with reduced M2-like MDMs and increased M1-like MDMs and $CD8^+$ T cells in the TME, indicating that this peptide can modify CHI3L1 protein complexes and thereby reprogram the immune microenvironment. Although $CD8^+$ T cells were significantly increased by GMP treatment, we observed elevated levels of CTLA-4 and PD-1 expression in these T cells, a hallmark feature of T-cell exhaustion, suggesting that GMP may synergize with immune checkpoint inhibitors to form more effective immunotherapy for GBM treatment. Based on analyzing a publicly available clinical dataset (41), the higher and lower levels of *LGALS3BP* combined with *LGALS3* or *CHI3L1* gene expression are associated with response to anti-PD-1 immunotherapy, reinforcing the mechanism of CHI3L1-Gal3/Gal3BP protein complexes in regulating protumor or antitumor immunity in GBM. In summary, the findings in this study shed light on a crucial molecular mechanism of macrophage-mediated immunosuppression in GBM, indicating the development of a more effective treatment for patients with this devasting brain cancer.

Methods

Detailed methods can be found in the supplemental material.

Cell lines. GBM patient-derived neurosphere lines (TS543, TS603, BT112) and human neural stem cell lines (hNSCs) were used and cultured as described previously (14). Mouse glioma cell line QPP7 provided by Dr. Jian Hu (MD Anderson Cancer Center, Houston, TX) was cultured in the serum-free NSC medium. U87, GL261, RAW246.7, and 293T from ATCC were cultured in DMEM supplemented with 10% FBS (Sigma-Aldrich,) and penicillin/streptomycin (P/S) (Gibco). SIM-A9 from ATCC was cultured in DMEM/F12 supplemented with 10% FBS, 5% horse serum, and P/S. THP-1 cell line was purchased from ATCC and cultured in RPMI-1640 supplemented with 10% FBS, 0.05 mM 2-mercaptoethanol, and P/S. All cell lines were verified to be mycoplasma-free using MyCoAlert PLUS Mycoplasma Detection Kit (Lonza, Cat# LT07-710), and cultured at 37°C with 5% CO_2.

BMDM culture and polarization. BMDMs were isolated from male and female C57BL/6 mice as previously described (26). Briefly, femur bones were isolated from mice, and IMDM (ATCC) supplemented with 10% FBS and P/S was used to flush the bone marrow into a petri dish. After 4-6-hour incubation, the floating cells were collected and resuspended in the medium with 20 ng/mL M-CSF (PrproTech). On day 6, the fully differentiated cells were designated as an M0 state. To induce BMDM polarization toward an M1 state, 100 ng/mL LPS (Invitrogen) and 50 ng/mL IFNγ (PrproTech) were added to the M0 cells for 24 hours. To induce BMDM polarization toward an M2 state, 20 ng/mL IL-4 (PrproTech) was added to the M0 cells for 72 hours.

Intracranial xenograft tumor models, macrophage depletion, T cell depletion, and peptide treatment. Male and female ICR SCID and C57BL/6 mice (4-6 weeks of age) were purchased from Taconic Biosciences and The Jackson Laboratory, respectively. The intracranial xenograft tumor models were established as previously described (14). Cells in 5 µL DPBS were injected at the following numbers: TS543 vector control or CHI3L1 overexpression (OE), 1×10^4 cells; QPP7 scrambled control or CHI3L1 knockdown (KD), 1×10^5 cells; and GL261 vector control or CHI3L1 OE, 1×10^5 cells. For tumor models with macrophage depletion, Chodrosome or control liposome (Clodrosome, Cat# CLD-8901) was injected into animals through the tail vein. For tumor models with T cell depletion, IgG (BioXCell, Cat# BE0090) or anti-CD4 (BioXCell, Cat# BE0003-1) and anti-CD8 (BioXCell, Cat# BE0061) antibodies were injected into animals through intraperitoneal injection. For mice treated

with peptides, 5 uL of 20 uM SCP or GMP was delivered into the mouse brain every 4 days with a total of seven times.

Enzyme-linked immunosorbent assay (ELISA). Secreted CHI3L1 protein in the cell culture supernatant was measured by using the Quantikine Human CHI3L1 Immunoassay (R&D Systems, Cat# DC3L10). CHI3L1 content in the conditioned media was quantified per million cells and no CHI3L1 was detected in DMEM or NSC medium supplemented with EGF and bFGF.

Co-Immunoprecipitation (Co-IP) and mass spectrometry (MS). TS603 cells overexpressing CHI3L1 with V5 tag (TS603 CHI3L1_V5_OE) or THP-1 cells treated with the peptides were collected and protein-protein interaction was crosslinked with 2 mM Dithiobis (succinimidyl propionate, DSP). Membrane proteins were extracted with the Membrane Protein Extraction Kit (ThermoFisher, Cat# 89842) and ~ 500 µg of protein was used for Co-IP assay by the Co-Immunoprecipitation Kit (ThermoFisher, Cat# 26149). For mass spectrometry, 10 µg of each of the TS603 CHI3L1_V5_OE Co-IP samples were separated in a 12% SDS-PAGE gel and analyzed by MS at the University of Pittsburgh Biomedical MS Center.

Immunoblotting (IB), Immunohistochemistry (IHC), and Immunofluorescence (IF). Cells were lysed on ice using RIPA buffer (Millipore) supplemented with protease and phosphatase inhibitors (Roche). The protein concentration was determined by the BCA method and 15~30 ug of total proteins were loaded and analyzed by Western blotting with indicated antibodies. For IHC staining, brain tissues were fixed in 10% formalin overnight and embedded in paraffin. For IF staining, fresh brain tissues were immediately frozen in OCT on dry ice. IHC and IF staining were performed as we described previously (14). Additional information about antibodies is provided in the Supplementary Material and Methods section.

Scratch-wound healing assay. BMDM were polarized to the indicated status (M0, M1, or M2) and seeded in 12-well plates at 80-90% confluency. The cells were switched to the medium without FBS for 6 hours of starvation. Scratches were made using pipettor tips and fresh IMDM with indicated recombinant proteins and/or peptides were added. Images of the scratches were captured at indicated times. For the SIM-A9 scratch-wound healing assay, 12-well plates were coated with 10 µg/mL fibronectin (Sigma-Aldrich) at 37 °C overnight before seeding cells.

Transwell migration assay. Polarized BMDMs were starved by removing FBS for 6 hours. Cells were collected and 2×10^5 cells in 200 µL of IMDM were added into each transwell insert (Millipore, Cat# MCMP24H48). 700 µL of IMDM containing 2% FBS and the indicated recombinant proteins was added to the bottom of the plates. After 14-hour incubation, transwell inserts were stained with HEMA 3 Stain Set (Fisher Scientific). Insert membranes were separated and mounted on glass slides with CYTOSEAL XYL (ThermoFisher) and images were taken by an inverted microscope (Leica DM 2500). For the SIM-A9 cells, the inserts were coated with 10 µg/mL fibronectin overnight in advance of seeding cells.

RNA isolation, qRT-PCR, and RNA-seq. RNA was extracted and cDNA was synthesized as described previously (14). qRT-PCR was performed using PowerSYBR Green PCR Master Mix (Applied Biosystems) and detected with a StepOnePlus Real-Time PCR System (Applied Biosystems). Primers are listed in **Supplementary Table S3**. Each reaction was performed in duplicate or triplicate. The relative expression of genes was normalized to human RPL39 or mouse 18S ribosomal RNA. For RNA-seq experiments, cells from intracranial xenograft tumors were isolated and incubated with antibodies for immune cell types. Macrophages were isolated by FACS and RNA was then isolated and sent to Health Sciences Sequencing Core at UPMC Children's Hospital of Pittsburgh for RNA-seq. RNA-seq data are available in the NCBI's GEO (accession number GSE174177).

MRI and bioluminescent Imaging. MRI and bioluminescent imaging of mice were performed at Rangos Research Center Animal Imaging Core. The tumor size of mice detected by MRI was analyzed with ITK-SNAP. For bioluminescent imaging, mice were intraperitoneally injected with D-Luciferin (150 mg/Kg; GoldBio), and images were captured by the IVIS Lumina S5 system (PerkinElmer).

Brain tumor cell isolation. Mice with neurological deficits or moribund appearance were sacrificed. Tumors were separated and homogenized for 15 min at 37°C in Collagenase IV Cocktail (3.2 mg/mL collagenase type IV, 2 mg/mL soybean trypsin inhibitor, and 1.0 mg/mL deoxyribonuclease I; Worthington Biochemical). Red blood cells were lysed using ACK lysing buffer (Gibco). Cell suspensions were filtered through 70-µm strainers, centrifuged, and resuspended in cold FACS buffer (DPBS with 1% BSA) for further analysis.

Flow cytometry and CyTOF. About 3×10^6 cells were used for each staining panel. Cells were incubated with 1.0 µg of TruStain fcX (BioLegend) for 10 min on ice to block Fc receptors, followed by staining with the combination of indicated antibodies. After staining, cells were washed with FACS buffer three times and

incubated with Fixation Buffer (BioLegend) at RT for 20 min. Cells were washed with FACS buffer, resuspended in Cyto-Last Buffer (BioLegend), and analyzed by either a BD LSRFortessa or BD FACSAria II SORP**.** For CyTOF, samples were prepared as described above for flow cytometry. Three pairs of samples (scrambled shRNA *vs Chi3l1* KD) with similar tumor sizes were chosen and the staining procedure was followed as previously described (51). The samples were analyzed on a Helios2 CyTOF system (Fluidigm) at the Longwood Medical Area CyTOF Core. Additional information about flow cytometry antibodies is provided in the Supplementary Material and Methods section.

Structure analysis of protein-protein interaction. Prediction of protein-protein interaction was based on available human protein structures for binding of CHI3L1 and other putative protein candidates. Protein structures of CHI3L1 (PDB 1HJV), Gal3 (PDB 6FOF), and Gal3BP monomer (PDB 6GFB) were used for protein-protein interaction analyses. Docked poses of CHI3L1 with Gal3BP (monomer of dimerization domain) and CHI3L1 with Gal3 were predicted using ClusPro (52) and further analyzed with FastContact for energetic complementarity (33).

Peptide design. GMP was designed using molecular dynamics (MD) simulations in AMBER18 on the GPU-accelerated code with AMBER ff14SB force field (53, 54). The tLeap binary was used to solve structures in an octahedral TIP3P water box with a 15 Å distance from the peptide surface to the box edges and a closeness parameter of 0.75 Å. The system was neutralized and solvated in 150 mM NaCl. The non-bonded interaction cutoff was set to 8 Å. Hydrogen bonds were constrained using the SHAKE algorithm and an integration time step of 2 fs. Simulations were carried out by equilibrating the system for 5 ns at NPT, using a Berendsen thermostat to maintain a constant pressure of 1 atm followed by 300 ns NVT production at 300 K.

Data analysis. Data are calculated with GraphPad Prism and presented as the mean ± SD or ± SEM. $P < 0.05$ was considered as the statistical significance and it was determined by the indicated tests in figure legends. Scratch-wound healing areas of cell migration, Transwell migration assay cell number, and IF staining positive cells were analyzed by using Fiji software (ImageJ). Flow cytometry data were gated, analyzed, and visualized using FlowJo software (BD). CyTOF data were analyzed with Cytobank (Cytobank Inc.). TCGA GBM datasets were used for clinical GBM analysis, and RNA-seq data (41) were used for correlation analysis between gene expression (*CHI3L1*, *LGALS3*, and *LGALS3BP*) and GBM patient response to anti-PD-1 treatment.

Study approval. All animal experiments were performed with the approval of the University of Pittsburgh's Institutional Animal Care and Use Committee (IACUC) (Protocol # 18031339, #21049271).

Author Contributions

A.C. and B.H. contributed to the conception and design of the study. A.C., Y.J., Z.L., V.S., Y.G., and J. M. performed experiments. U.S. and C.J.C. contributed to protein-protein interaction prediction and peptide design. L.W., H.Z, C.C., S.L., X.L., and Q.W. contributed to bioinformatics analysis for RNA-seq, TCGA datasets, and clinical datasets. A.C. and B.H. analyzed, interpreted data, and wrote the original manuscript. J.M., Y.W., Y.S., D.Y., L.K., N.A., P.Z., G.K., S.A., D.S., G.G., and X.X. provided resources and technical supports. A.C., L.M.M., C.J.C., D.Y., I.F.P., and B.H. reviewed and edited the manuscript.

Acknowledgments

The authors would like to thank Dr. Ronald A DePinho for critically evaluating the manuscript; Drs. Jiangong Ren and Jian Hu from UT Texas MD Anderson Cancer Center for providing the mouse glioma cell line QPP7; Drs. Junfei Zhao and Raul Rabadan from Columbia University for providing detailed information about their published RNA-seq datasets; Samuel K Wyman and Jackson E Landman from Rangos Research Center Animal Imaging Core for assistance with MRI imaging; Drs. Nathan A Yates and Xuemei Zeng from BioMS Center for assistance with mass spectrometry experiments; Dr. William A MacDonald from Health Sciences Sequencing Core for assistance with RNA sequencing; Dr. Krishna Prasadan from Rangos Research Center Cell Imaging Core for assistance with the confocal image; Drs. Esther P Jane and Daniel R Premkumar for sharing antibodies and reagents. This work was supported by the Scientific Program Fund from the Children's Hospital of Pittsburgh (B.Hu and I. F. Pollack.), the Translational Brain Tumor Research Fund (I. F. Pollack.), the Walter L. Copeland Fund of the Pittsburgh Foundation (B.Hu), and the Connor's Cure Fund from the V Foundation (B.Hu and I. F. Pollack).

References

1. Wen PY, and Kesari S. Malignant gliomas in adults. *N Engl J Med.* 2008;359(5):492-507.
2. Desjardins A. Neuro-oncology: What is the optimal use of bevacizumab in glioblastoma? *Nat Rev Neurol.* 2015.
3. Furnari FB, Fenton T, Bachoo RM, Mukasa A, Stommel JM, Stegh A, et al. *Genes Dev*. 2007:2683-710.
4. Buerki RA, Chheda ZS, and Okada H. Immunotherapy of Primary Brain Tumors: Facts and Hopes. *Clin Cancer Res.* 2018;24(21):5198-205.
5. Lim M, Xia Y, Bettegowda C, and Weller M. Current state of immunotherapy for glioblastoma. *Nat Rev Clin Oncol.* 2018;15(7):422-42.
6. Sampson JH, Gunn MD, Fecci PE, and Ashley DM. Brain immunology and immunotherapy in brain tumours. *Nat Rev Cancer.* 2020;20(1):12-25.
7. Hambardzumyan D, Gutmann DH, and Kettenmann H. The role of microglia and macrophages in glioma maintenance and progression. *Nat Neurosci.* 2016;19(1):20-7.
8. Ginhoux F, Greter M, Leboeuf M, Nandi S, See P, Gokhan S, et al. Fate mapping analysis reveals that adult microglia derive from primitive macrophages. *Science.* 2010;330(6005):841-5.
9. Chen Z, Feng X, Herting CJ, Garcia VA, Nie K, Pong WW, et al. Cellular and Molecular Identity of Tumor-Associated Macrophages in Glioblastoma. *Cancer Res.* 2017;77(9):2266-78.
10. Pinton L, Masetto E, Vettore M, Solito S, Magri S, D'Andolfi M, et al. The immune suppressive microenvironment of human gliomas depends on the accumulation of bone marrow-derived macrophages in the center of the lesion. *J Immunother Cancer.* 2019;7(1):58.
11. Komohara Y, Ohnishi K, Kuratsu J, and Takeya M. Possible involvement of the M2 anti-inflammatory macrophage phenotype in growth of human gliomas. *J Pathol.* 2008;216(1):15-24.
12. Wang Q, Hu B, Hu X, Kim H, Squatrito M, Scarpace L, et al. Tumor Evolution of Glioma-Intrinsic Gene Expression Subtypes Associates with Immunological Changes in the Microenvironment. *Cancer Cell.* 2017;32(1):42-56 e6.
13. Quail DF, and Joyce JA. The Microenvironmental Landscape of Brain Tumors. *Cancer Cell.* 2017;31(3):326-41.

14. Hu B, Wang Q, Wang YA, Hua S, Sauve CG, Ong D, et al. Epigenetic Activation of WNT5A Drives Glioblastoma Stem Cell Differentiation and Invasive Growth. *Cell.* 2016;167(5):1281-95 e18.
15. Fusetti F, Pijning T, Kalk KH, Bos E, and Dijkstra BW. Crystal structure and carbohydrate-binding properties of the human cartilage glycoprotein-39. *J Biol Chem.* 2003;278(39):37753-60.
16. Lee CG, Da Silva CA, Dela Cruz CS, Ahangari F, Ma B, Kang MJ, et al. Role of chitin and chitinase/chitinase-like proteins in inflammation, tissue remodeling, and injury. *Annu Rev Physiol.* 2011;73:479-501.
17. Iwamoto FM, Hottinger AF, Karimi S, Riedel E, Dantis J, Jahdi M, et al. Serum YKL-40 is a marker of prognosis and disease status in high-grade gliomas. *Neuro Oncol.* 2011;13(11):1244-51.
18. Pelloski CE, Mahajan A, Maor M, Chang EL, Woo S, Gilbert M, et al. YKL-40 expression is associated with poorer response to radiation and shorter overall survival in glioblastoma. *Clin Cancer Res.* 2005;11(9):3326-34.
19. Darmanis S, Sloan SA, Croote D, Mignardi M, Chernikova S, Samghababi P, et al. Single-Cell RNA-Seq Analysis of Infiltrating Neoplastic Cells at the Migrating Front of Human Glioblastoma. *Cell Rep.* 2017;21(5):1399-410.
20. Shingu T, Ho AL, Yuan L, Zhou X, Dai C, Zheng S, et al. Qki deficiency maintains stemness of glioma stem cells in suboptimal environment by downregulating endolysosomal degradation. *Nat Genet.* 2016.
21. Genoud V, Marinari E, Nikolaev SI, Castle JC, Bukur V, Dietrich PY, et al. Responsiveness to anti-PD-1 and anti-CTLA-4 immune checkpoint blockade in SB28 and GL261 mouse glioma models. *Oncoimmunology.* 2018;7(12):e1501137.
22. Kawada M, Seno H, Kanda K, Nakanishi Y, Akitake R, Komekado H, et al. Chitinase 3-like 1 promotes macrophage recruitment and angiogenesis in colorectal cancer. *Oncogene.* 2012;31(26):3111-23.
23. Xu N, Bo Q, Shao R, Liang J, Zhai Y, Yang S, et al. Chitinase-3-Like-1 Promotes M2 Macrophage Differentiation and Induces Choroidal Neovascularization in Neovascular Age-Related Macular Degeneration. *Invest Ophthalmol Vis Sci.* 2019;60(14):4596-605.
24. Haynes SE, Hollopeter G, Yang G, Kurpius D, Dailey ME, Gan WB, et al. The P2Y12 receptor regulates microglial activation by extracellular nucleotides. *Nat Neurosci.* 2006;9(12):1512-9.

25. Butovsky O, Jedrychowski MP, Moore CS, Cialic R, Lanser AJ, Gabriely G, et al. Identification of a unique TGF-beta-dependent molecular and functional signature in microglia. *Nat Neurosci.* 2014;17(1):131-43.
26. Ying W, Cheruku PS, Bazer FW, Safe SH, and Zhou B. Investigation of macrophage polarization using bone marrow derived macrophages. *J Vis Exp.* 2013(76).
27. Chen B, Khodadoust MS, Liu CL, Newman AM, and Alizadeh AA. Profiling Tumor Infiltrating Immune Cells with CIBERSORT. *Methods Mol Biol.* 2018;1711:243-59.
28. Muller S, Kohanbash G, Liu SJ, Alvarado B, Carrera D, Bhaduri A, et al. Single-cell profiling of human gliomas reveals macrophage ontogeny as a basis for regional differences in macrophage activation in the tumor microenvironment. *Genome Biol.* 2017;18(1):234.
29. Loimaranta V, Hepojoki J, Laaksoaho O, and Pulliainen AT. Galectin-3-binding protein: A multitask glycoprotein with innate immunity functions in viral and bacterial infections. *J Leukoc Biol.* 2018;104(4):777-86.
30. MacKinnon AC, Farnworth SL, Hodkinson PS, Henderson NC, Atkinson KM, Leffler H, et al. Regulation of alternative macrophage activation by galectin-3. *J Immunol.* 2008;180(4):2650-8.
31. Sano H, Hsu DK, Yu L, Apgar JR, Kuwabara I, Yamanaka T, et al. Human galectin-3 is a novel chemoattractant for monocytes and macrophages. *J Immunol.* 2000;165(4):2156-64.
32. Inohara H, Akahani S, Koths K, and Raz A. Interactions between galectin-3 and Mac-2-binding protein mediate cell-cell adhesion. *Cancer Res.* 1996;56(19):4530-4.
33. Champ PC, and Camacho CJ. FastContact: a free energy scoring tool for protein-protein complex structures. *Nucleic Acids Res.* 2007;35(Web Server issue):W556-60.
34. Pyonteck SM, Akkari L, Schuhmacher AJ, Bowman RL, Sevenich L, Quail DF, et al. CSF-1R inhibition alters macrophage polarization and blocks glioma progression. *Nat Med.* 2013;19(10):1264-72.
35. Kaneda MM, Messer KS, Ralainirina N, Li H, Leem CJ, Gorjestani S, et al. PI3Kgamma is a molecular switch that controls immune suppression. *Nature.* 2016;539(7629):437-42.
36. van Rooijen N, Kors N, ter Hart H, and Claassen E. In vitro and in vivo elimination of macrophage tumor cells using liposome-encapsulated dichloromethylene diphosphonate. *Virchows Arch B Cell Pathol Incl Mol Pathol.* 1988;54(4):241-5.

37. Fulci G, Dmitrieva N, Gianni D, Fontana EJ, Pan X, Lu Y, et al. Depletion of peripheral macrophages and brain microglia increases brain tumor titers of oncolytic viruses. *Cancer Res.* 2007;67(19):9398-406.
38. Woroniecka K, Chongsathidkiet P, Rhodin K, Kemeny H, Dechant C, Farber SH, et al. T-Cell Exhaustion Signatures Vary with Tumor Type and Are Severe in Glioblastoma. *Clin Cancer Res.* 2018;24(17):4175-86.
39. Medikonda R, Dunn G, Rahman M, Fecci P, and Lim M. A review of glioblastoma immunotherapy. *J Neurooncol.* 2020.
40. Topalian SL, Drake CG, and Pardoll DM. Immune checkpoint blockade: a common denominator approach to cancer therapy. *Cancer Cell.* 2015;27(4):450-61.
41. Zhao J, Chen AX, Gartrell RD, Silverman AM, Aparicio L, Chu T, et al. Immune and genomic correlates of response to anti-PD-1 immunotherapy in glioblastoma. *Nat Med.* 2019;25(3):462-9.
42. Wellenstein MD, and de Visser KE. Cancer-Cell-Intrinsic Mechanisms Shaping the Tumor Immune Landscape. *Immunity.* 2018;48(3):399-416.
43. Novak R, Dabelic S, and Dumic J. Galectin-1 and galectin-3 expression profiles in classically and alternatively activated human macrophages. *Biochim Biophys Acta.* 2012;1820(9):1383-90.
44. Gleissner CA, Erbel C, Linden F, Domschke G, Akhavanpoor M, Helmes CM, et al. Galectin-3 binding protein, coronary artery disease and cardiovascular mortality: Insights from the LURIC study. *Atherosclerosis.* 2017;260:121-9.
45. Shaked I, Hanna DB, Gleissner C, Marsh B, Plants J, Tracy D, et al. Macrophage inflammatory markers are associated with subclinical carotid artery disease in women with human immunodeficiency virus or hepatitis C virus infection. *Arterioscler Thromb Vasc Biol.* 2014;34(5):1085-92.
46. Tomaszewski W, Sanchez-Perez L, Gajewski TF, and Sampson JH. Brain Tumor Microenvironment and Host State: Implications for Immunotherapy. *Clin Cancer Res.* 2019;25(14):4202-10.
47. Jackson CM, Choi J, and Lim M. Mechanisms of immunotherapy resistance: lessons from glioblastoma. *Nat Immunol.* 2019;20(9):1100-9.
48. Jallal B, Powell J, Zachwieja J, Brakebusch C, Germain L, Jacobs J, et al. Suppression of tumor growth in vivo by local and systemic 90K level increase. *Cancer Res.* 1995;55(15):3223-7.

49. Ullrich A, Sures I, D'Egidio M, Jallal B, Powell TJ, Herbst R, et al. The secreted tumor-associated antigen 90K is a potent immune stimulator. *J Biol Chem.* 1994;269(28):18401-7.

50. Kalayci O, Birben E, Tinari N, Oguma T, Iacobelli S, and Lilly CM. Role of 90K protein in asthma and TH2-type cytokine expression. *Ann Allergy Asthma Immunol.* 2004;93(5):485-92.

51. Mitsialis V, Wall S, Liu P, Ordovas-Montanes J, Parmet T, Vukovic M, et al. Single-Cell Analyses of Colon and Blood Reveal Distinct Immune Cell Signatures of Ulcerative Colitis and Crohn's Disease. *Gastroenterology.* 2020;159(2):591-608 e10.

52. Comeau SR, Gatchell DW, Vajda S, and Camacho CJ. ClusPro: a fully automated algorithm for protein-protein docking. *Nucleic Acids Res.* 2004;32(Web Server issue):W96-9.

53. Salomon-Ferrer R, Gotz AW, Poole D, Le Grand S, and Walker RC. Routine Microsecond Molecular Dynamics Simulations with AMBER on GPUs. 2. Explicit Solvent Particle Mesh Ewald. *J Chem Theory Comput.* 2013;9(9):3878-88.

54. Maier JA, Martinez C, Kasavajhala K, Wickstrom L, Hauser KE, and Simmerling C. ff14SB: Improving the Accuracy of Protein Side Chain and Backbone Parameters from ff99SB. *J Chem Theory Comput.* 2015;11(8):3696-713.

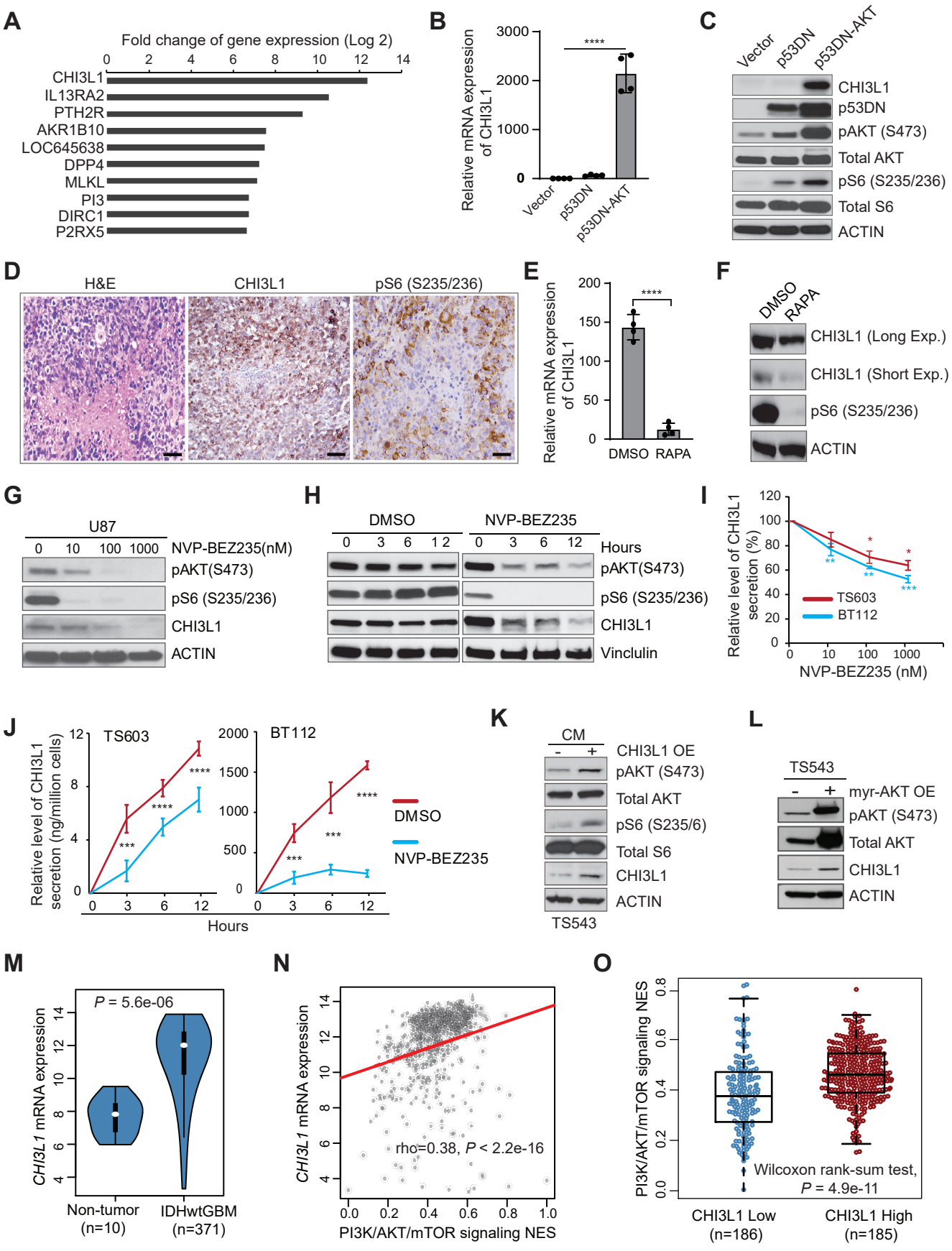
A
Fold change of gene expression (Log 2)
0 2 4 6 8 10 12 14
CHI3L1
IL13RA2
PTH2R
AKR1B10
LOC645638
DPP4
MLKL
PI3
DIRC1
P2RX5
B
Relative mRNA expression of CHI3L1
3000
2000
1000
0
****
Vector
p53DN
p53DN-AKT
C
Vector
p53DN
p53DN-AKT
CHI3L1
p53DN
pAKT (S473)
Total AKT
pS6 (S235/236)
Total S6
ACTIN
D
H&E
CHI3L1
pS6 (S235/236)
E
Relative mRNA expression of CHI3L1
200
150
100
50
0
****
DMSO
RAPA
F
DMSO
RAPA
CHI3L1 (Long Exp.)
CHI3L1 (Short Exp.)
pS6 (S235/236)
ACTIN
G
U87
0 10 100 1000
NVP-BEZ235(nM)
pAKT(S473)
pS6 (S235/236)
CHI3L1
ACTIN
H
DMSO
NVP-BEZ235
0 3 6 12
0 3 6 12
Hours
pAKT(S473)
pS6 (S235/236)
CHI3L1
Vinculin
I
Relative level of CHI3L1 secretion (%)
120
100
80
60
40
20
0
TS603
BT112
0 10 100 1000
NVP-BEZ235 (nM)
J
Relative level of CHI3L1 secretion (ng/million cells)
TS603
BT112
DMSO
NVP-BEZ235
Hours
0 3 6 12
K
CM
- +
CHI3L1 OE
pAKT (S473)
Total AKT
pS6 (S235/6)
Total S6
CHI3L1
ACTIN
TS543
L
TS543
- +
myr-AKT OE
pAKT (S473)
Total AKT
CHI3L1
ACTIN
M
P = 5.6e-06
CHI3L1 mRNA expression
Non-tumor (n=10)
IDHwtGBM (n=371)
N
CHI3L1 mRNA expression
rho=0.38, P < 2.2e-16
PI3K/AKT/mTOR signaling NES
O
PI3K/AKT/mTOR signaling NES
Wilcoxon rank-sum test, P = 4.9e-11
CHI3L1 Low (n=186)
CHI3L1 High (n=185)

Figure Legends

Figure 1. CHI3L1 upregulation is associated with activation of the PI3K/AKT/mTOR signaling in GBM.

(**A**) Top 10 upregulated genes in hNSC *vs* hNSC-p53DN-AKT ranked by fold change of gene expression. qRT-PCR for CHI3L1 expression (**B**) and immunoblot analysis of indicated proteins (**C**) in hNSC expressing p53DN or/and myr-AKT. (**D**) Representative H&E and IHC images showing indicated proteins in tumors derived from hNSCs-p53DN-AKT. Scale bar, 50 μm. qRT-PCR (**E**) and immunoblot analysis (**F**) of indicated gene and proteins in hNSC-p53DN-AKT with rapamycin (RAPA) treatment (100 nM, 24 hours); CHI3L1 signal was shown in both long and short exposure time. Immunoblot analysis of indicated proteins in U87 treated with NVP-BEZ235 in a dose (**G**) and time (**H**) dependent manner. CHI3L1 secretion in the conditioned media (CM) was assessed by ELISA from human GBM neurosphere lines treated with NVP-BEZ235 at indicated concentrations after 12 hours of treatment (**I**) or at the concentration of 1 μM in indicated times (**J**). (**K**) Immunoblot analysis of indicated proteins in human GBM neurosphere line TS543 treated with CM of TS543 overexpressing (OE) CHI3L1 *vs* control (**K**) or overexpressing myr-AKT *vs* control (**L**). (**M**) *CHI3L1* mRNA expression in TCGA IDHwt GBM tumors compared to non-tumor brain tissues. Gene expression was normalized by RMA and the *P*-value was calculated by Wilcoxon rank-sum test. (**N**) Association between *CHI3L1* mRNA expression and the PI3K/AKT/mTOR signature score. Gene expression was normalized by RMA and *P*-value was calculated by Spearman rank correlation. (**O**) Enrichment of the PI3K/AKT/mTOR signature in IDHwt GBM with high and low levels of *CHI3L1* mRNA expression. Data are presented as the mean ± SD (n≥ 3 replicates); *P*-value was calculated using one-way ANOVA (**B**) or one-tailed unpaired *t* test (**E**, **I**, and **J**); $^{*}P < 0.05$, $^{**}P < 0.01$, $^{***}P < 0.001$, and $^{****}P < 0.0001$.

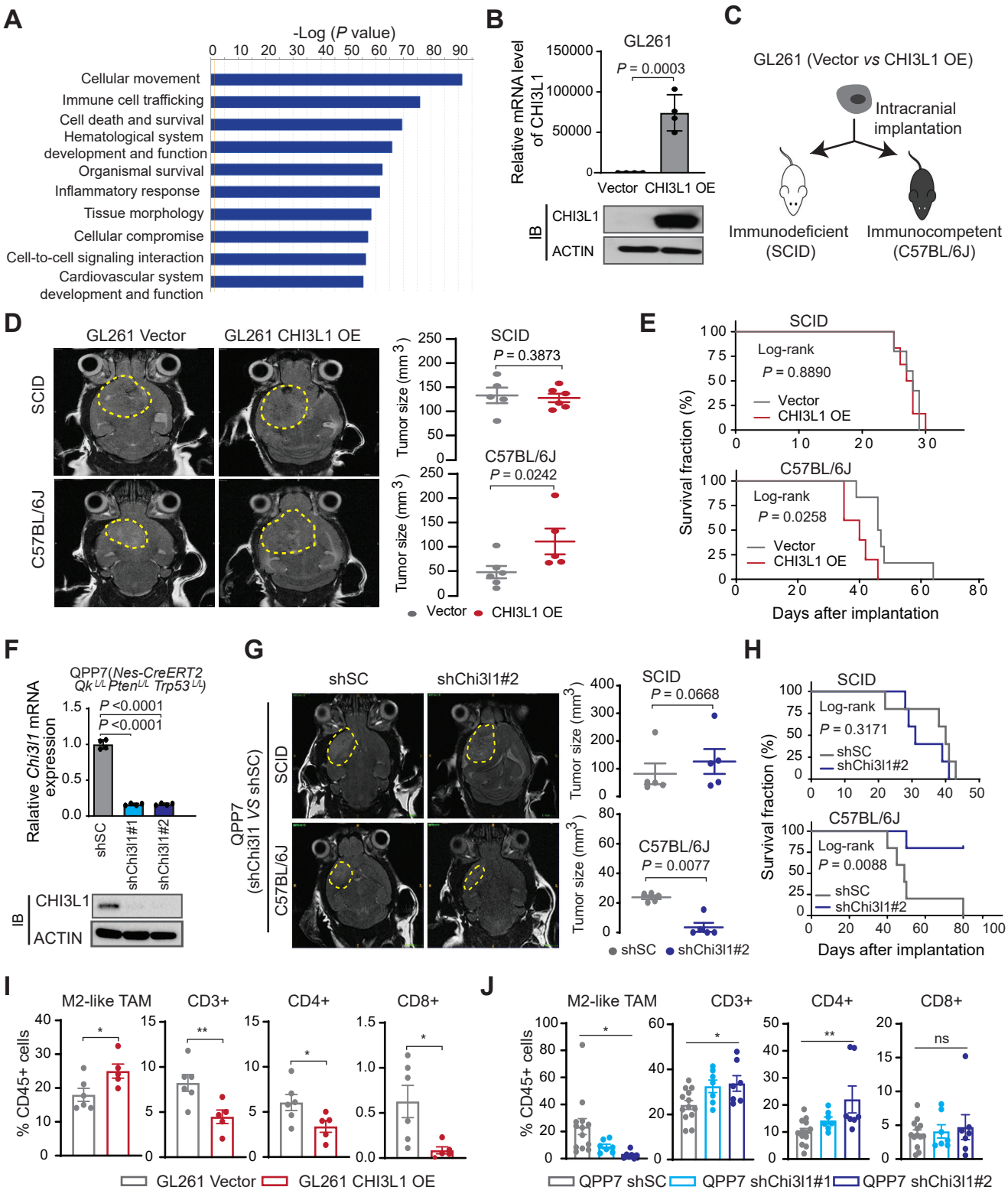
A
-Log (P value)
0 10 20 30 40 50 60 70 80 90
Cellular movement
Immune cell trafficking
Cell death and survival
Hematological system development and function
Organismal survival
Inflammatory response
Tissue morphology
Cellular compromise
Cell-to-cell signaling interaction
Cardiovascular system development and function
B
GL261
P = 0.0003
Relative mRNA level of CHI3L1
150000
100000
50000
0
Vector CHI3L1 OE
IB
CHI3L1
ACTIN
C
GL261 (Vector vs CHI3L1 OE)
Intracranial implantation
Immunodeficient (SCID)
Immunocompetent (C57BL/6J)
D
GL261 Vector
GL261 CHI3L1 OE
SCID
C57BL/6J
Tumor size (mm3)
SCID
P = 0.3873
C57BL/6J
P = 0.0242
Vector
CHI3L1 OE
E
SCID
Log-rank
P = 0.8890
Vector
CHI3L1 OE
C57BL/6J
Log-rank
P = 0.0258
Vector
CHI3L1 OE
Survival fraction (%)
Days after implantation
F
QPP7(Nes-CreERT2 Qk L/L Pten L/L Trp53 L/L)
Ralative Chi3l1 mRNA expression
P <0.0001
P <0.0001
shSC
shChi3l1#1
shChi3l1#2
IB
CHI3L1
ACTIN
G
shSC
shChi3l1#2
QPP7 (shChi3l1 VS shSC)
SCID
C57BL/6J
Tumor size (mm3)
SCID
P = 0.0668
C57BL/6J
P = 0.0077
shSC
shChi3l1#2
H
SCID
Log-rank
P = 0.3171
shSC
shChi3l1#2
C57BL/6J
Log-rank
P = 0.0088
shSC
shChi3l1#2
Survival fraction (%)
Days after implantation
I
M2-like TAM
CD3+
CD4+
CD8+
% CD45+ cells
GL261 Vector
GL261 CHI3L1 OE
J
M2-like TAM
CD3+
CD4+
CD8+
ns
% CD45+ cells
QPP7 shSC
QPP7 shChi3l1#1
QPP7 shChi3l1#2

Figure 2. Tumor progression and the immune microenvironment are implicated in glioma mouse models with alerting CHI3L1 expression.

(**A**) Top 10 biological functional pathways are enriched in CHI3L1 correlated genes in TCGA GBM datasets using the Ingenuity Pathway Analysis (IPA). (**B**) qRT-PCR and immunoblot analyses of the expression levels of CHI3L1 mRNA and protein in GL216 overexpressing (OE) vector control or human *CHI3L1* gene. Data are presented as the mean ± SD; *P*-value was calculated using a one-tailed unpaired *t* test. (**C**) Illustration of two orthotopic xenograft models with GL261 CHI3L1 OE or vector control. (**D**) Representative MRI from mice after intracranial injection of GL261 with CHI3L1 OE or Vector. T2 sequences demonstrate infiltrative tumors in the mouse brain (yellow line). Tumor volume was measured by the T2 MRI scan. (**E**) Kaplan–Meier tumor-free survival analysis of GL261 models. (**F**) qRT-PCR and immunoblot analyses of the expression levels of CHI3L1 mRNA and protein in QPP7 cells infected with lentivirus carrying shRNA targeting mouse *Chi3l1* gene (shChi3l1#1 and #2) *vs* shRNA scrambled controls (shSC). Data are presented as the mean ± SD; *P*-value was calculated by one-way ANOVA with Dunnett's multiple comparison test. (**G**) Representative MRI from two orthotopic xenograft glioma mouse models bearing QPP7 with shChi3l1#2 *vs* shSC. Tumor volume was measured by the T2 MRI scan. (**H**) Kaplan–Meier tumor-free survival analysis of QPP7 models. Flow cytometry analyses of the indicated cell populations in GL216 (**I**) and QPP7(**J**) syngeneic mouse models with altering CHI3L1 expression. The dots represent mice from the group; data are presented as the mean ± SEM; *P*-value was calculated using a one-tailed unpaired *t* test (**I**) or one-way ANOVA (**J**); $^{*}P < 0.05$, $^{**}P < 0.01$; ns represents no significance.

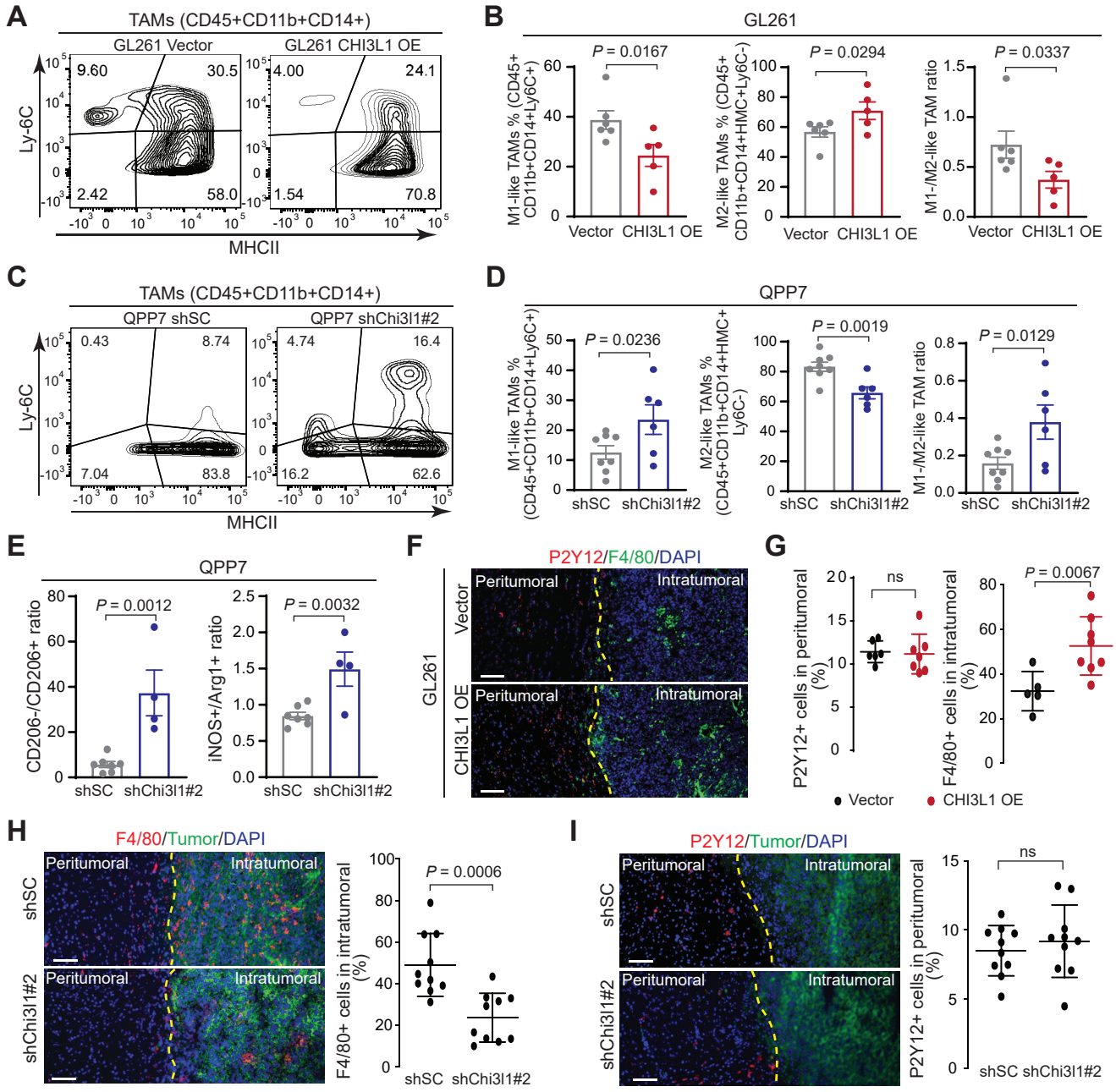
A
TAMs (CD45+CD11b+CD14+)
GL261 Vector
GL261 CHI3L1 OE
Ly-6C
MHCII
9.60
30.5
2.42
58.0
4.00
24.1
1.54
70.8
B
GL261
M1-like TAMs % (CD45+ CD11b+CD14+Ly6C+)
M2-like TAMs % (CD45+ CD11b+CD14+HMC+Ly6C-)
M1-/M2-like TAM ratio
P = 0.0167
P = 0.0294
P = 0.0337
Vector
CHI3L1 OE
C
TAMs (CD45+CD11b+CD14+)
QPP7 shSC
QPP7 shChi3l1#2
0.43
8.74
7.04
83.8
4.74
16.4
16.2
62.6
D
QPP7
M1-like TAMs % (CD45+CD11b+CD14+Ly6C+)
M2-like TAMs % (CD45+CD11b+CD14+HMC+ Ly6C-)
M1-/M2-like TAM ratio
P = 0.0236
P = 0.0019
P = 0.0129
shSC
shChi3l1#2
E
QPP7
CD206-/CD206+ ratio
iNOS+/Arg1+ ratio
P = 0.0012
P = 0.0032
F
P2Y12/F4/80/DAPI
GL261
Vector
CHI3L1 OE
Peritumoral
Intratumoral
G
P2Y12+ cells in peritumoral (%)
F4/80+ cells in intratumoral (%)
ns
P = 0.0067
Vector
CHI3L1 OE
H
F4/80/Tumor/DAPI
shSC
shChi3l1#2
F4/80+ cells in intratumoral (%)
P = 0.0006
I
P2Y12/Tumor/DAPI
P2Y12+ cells in peritumoral (%)
ns

Figure 3. CHI3L1 induces M2-like MDM accumulation *in vivo.*

Representative flow cytometry analyses and quantitation showing the percentage of M1- and M2-like MDMs in tumors derived from GL261 (**A** and **B**) and QPP7 (**C** and **D**) glioma-bearing mice with altering CHI3L1 expression. (**E**) The ratio of $CD206^-/CD206^+$ cells from the $CD45^+CD68^+CD11b^+$ cell population, and the ratio of $iNOS^+/Arg1^+$ cells from the $CD45^+$ cell population in QPP7-derived tumors. Each dot represents 1 mouse; data are presented as the mean ± SEM; *P*-value was calculated using a one-tailed unpaired *t* test. (**F**) Representative IF images for $F4/80^+$ and $P2Y12^+$ cells in tumor sections from the syngeneic mice bearing GL261-CHI3L1 *vs* vector control. (**G**) Quantitation of the indicated cells in peritumoral and intratumoral regions, respectively. Representative IF images and quantitation for $F4/80^+$ (**H**) and $P2Y12^+$ (**I**) cells in tumor sections from QPP7 glioma-bearing mice with shChi3l1#2 *vs* shSC. Peritumoral and intratumoral regions were separated using yellow lines. Each dot represents one field of the peritumoral or intratumoral region from indicated tumors (n≥3); Data are presented as the mean ± SD; *P*-value was calculated using a one-tailed unpaired *t* test; ns represents no significance; scale bar, 100 μm.

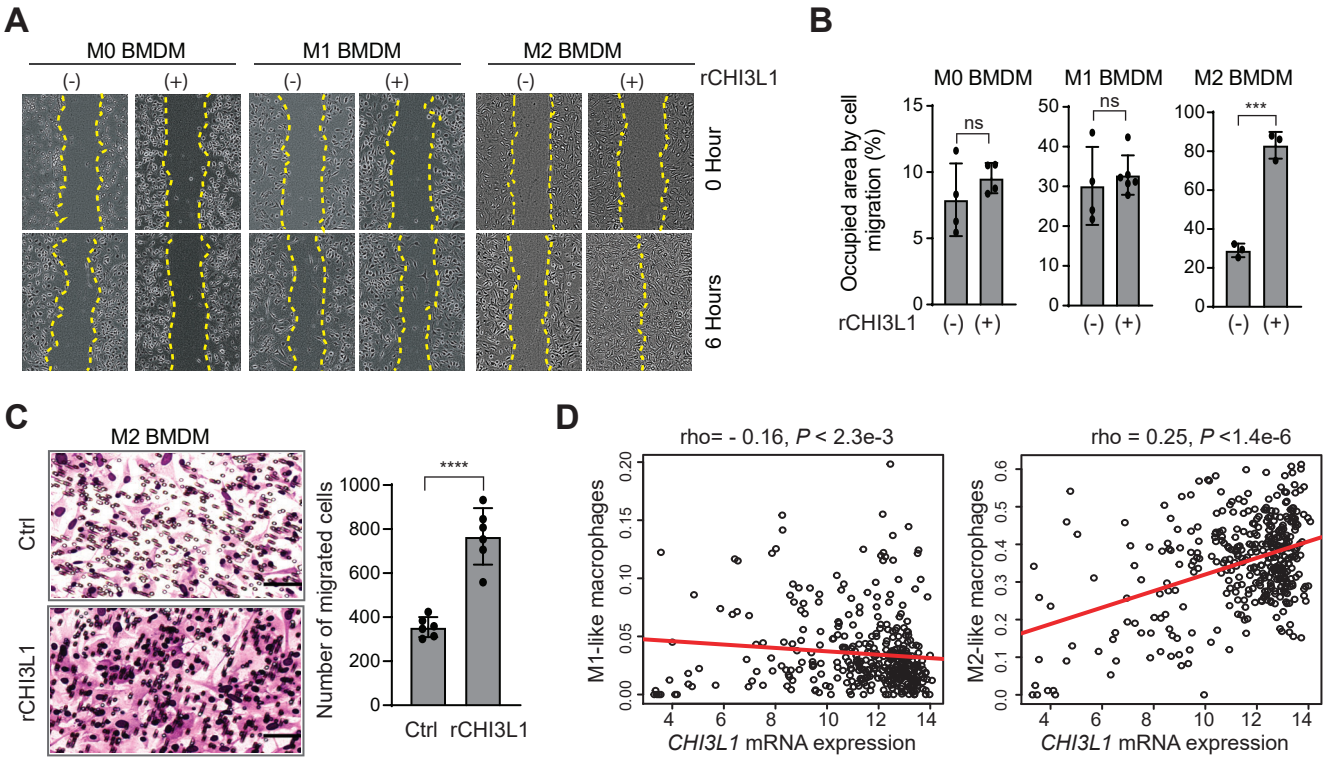
A
M0 BMDM
M1 BMDM
M2 BMDM
(-)
(+)
rCHI3L1
0 Hour
6 Hours
B
M0 BMDM
M1 BMDM
M2 BMDM
Occupied area by cell migration (%)
ns
ns
***
rCHI3L1
C
M2 BMDM
Ctrl
rCHI3L1
Number of migrated cells
****
Ctrl
rCHI3L1
D
rho= - 0.16, P < 2.3e-3
rho = 0.25, P <1.4e-6
M1-like macrophages
M2-like macrophages
CHI3L1 mRNA expression
CHI3L1 mRNA expression

Figure 4. CHI3L1 induces cell migration of M2-like MDM *in vitro.*

(**A**) Representative brightfield images showing cell migration in 0 and 6 hours after treatment with CHI3L1 recombinant protein (rCHI3L1) at the concentration of 0.6 μg/mL in M0, M1, and M2 BMDMs by the scratch-wound healing assay. (**B**) Cell migration was assessed by quantifying occupied areas by migrated cells. (**C**) Representative brightfield images for cell migration of M2 BMDMs by the Transwell assay. Migration was assessed by determining the number of migrated cells. Data are presented as the mean ± SD from at least three independent experiments; *P*-value was calculated using a one-tailed unpaired *t* test; $^{***}P < 0.001$, $^{****}P < 0.0001$; ns represents no significance. (**D**) Association between *CHI3L1* mRNA expression and M1/M2-like macrophage scores in IDHwt GBM. Gene expression was normalized by RMA and *P*-value was calculated by Spearman rank correlation.

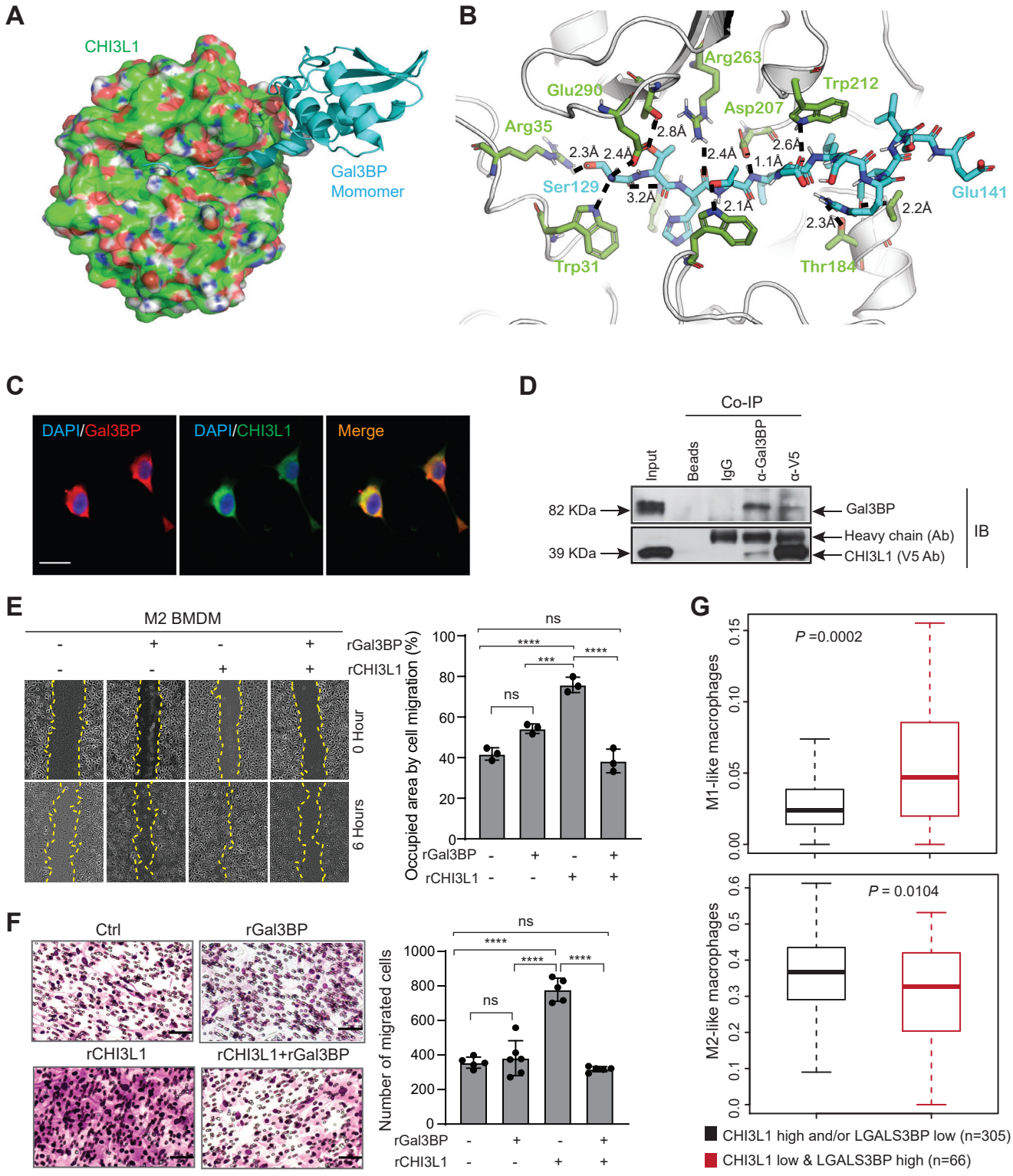
A
CHI3L1
Gal3BP
Momomer
B
Arg263
Glu290
Trp212
Asp207
Arg35
2.8Å
2.3Å
2.4Å
2.4Å
2.6Å
1.1Å
Ser129
3.2Å
2.1Å
2.2Å
2.3Å
Glu141
Trp31
Thr184
C
DAPI/Gal3BP
DAPI/CHI3L1
Merge
D
Co-IP
Input
Beads
IgG
α-Gal3BP
α-V5
82 KDa
39 KDa
Gal3BP
Heavy chain (Ab)
CHI3L1 (V5 Ab)
IB
E
M2 BMDM
rGal3BP
rCHI3L1
0 Hour
6 Hours
Occupied area by cell migration (%)
ns
****
***
F
Ctrl
rGal3BP
rCHI3L1
rCHI3L1+rGal3BP
Number of migrated cells
G
P =0.0002
M1-like macrophages
P = 0.0104
M2-like macrophages
CHI3L1 high and/or LGALS3BP low (n=305)
CHI3L1 low & LGALS3BP high (n=66)

Figure 5. Gal3BP interacts with CHI3L1 for inhibition of BMDM migration *in vitro.*

(**A**) A binding model of Gal3BP monomer (cyan from PDB 6GFB) and CHI3L1 (green surface with red/blue/white shades corresponding to O/N/H atoms from PDB 1HJV_A). (**B**) Detailed view from (**A**) of the binding mode of Ser129-Glu141 of Gal3BP (cyan) and CHI3L1 (green). The 10 hydrogen bonds are indicated with dashed lines and distances. Several hydrophobic contacts are also shown in the protein binding complex. (**C**) Representative IF images showing co-localization of proteins in TS603 cells; scale bar, 20 μm. (**D**) Immunoblot (IB) analysis of protein binding complexes after Co-IP with indicated antibodies in TS603 overexpressing V5-tagged CHI3L1. (**E**) Representative brightfield images from the scratch-wound healing assay showing M2 BMDM cell migration in 0 and 6 hours after treatment with recombinant CHI3L1protein (rCHI3L1, 2.5 μg/mL) and/or recombinant Gal3BP protein (rGal3BP, 5.0 μg/mL). Cell migration was assessed by quantifying occupied areas by migrated cells. (**F**) Representative brightfield images from the Transwell assay for M2 BMDM cell migration under treatment with rCHI3L1 (2.5 μg/mL) and/or rGal3BP (5.0 μg/mL). Migration was assessed by determining the number of migrated cells. In (**E**) and (**F**), data are presented as the mean ± SD from at least three independent experiments. *P*-value was calculated using one-way ANOVA with Tukey's multiple comparison test; $^{***}P < 0.001$; $^{****}P < 0.0001$; ns represents no significance; scale bar, 50 μm. (**G**) Boxplots showing enrichment of M1/M2-like macrophage signature in two indicated groups of TCGA GBMs. *P*-value was calculated by Wilcoxon rank-sum test.

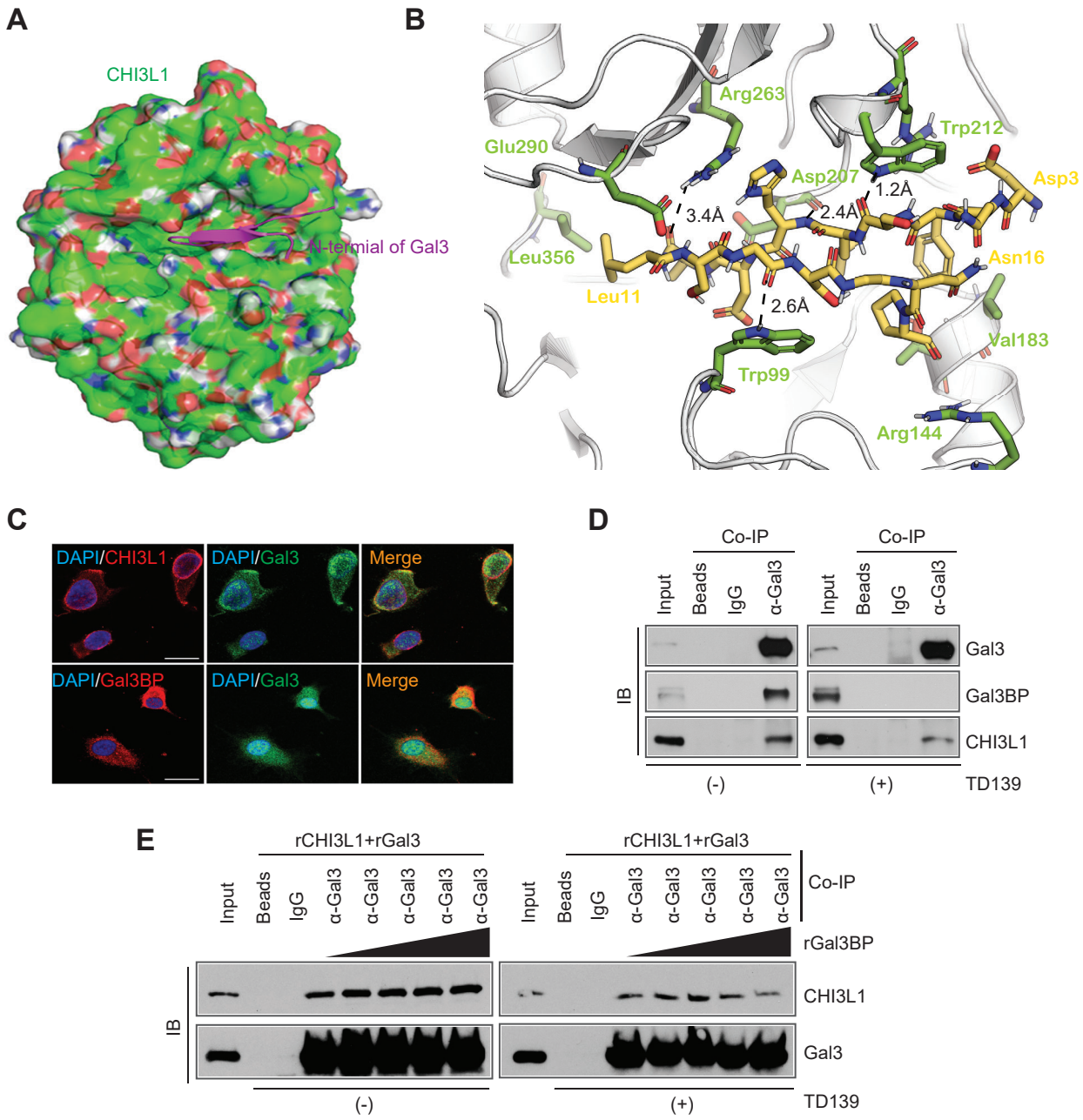
A
CHI3L1
N-termial of Gal3
B
Arg263
Trp212
Glu290
Asp207
Asp3
1.2Å
3.4Å
2.4Å
Leu356
Asn16
Leu11
2.6Å
Val183
Trp99
Arg144
C
DAPI/CHI3L1
DAPI/Gal3
Merge
DAPI/Gal3BP
DAPI/Gal3
Merge
D
Co-IP
Co-IP
Input
Beads
IgG
α-Gal3
Input
Beads
IgG
α-Gal3
IB
Gal3
Gal3BP
CHI3L1
(-)
(+)
TD139
E
rCHI3L1+rGal3
rCHI3L1+rGal3
Input
Beads
IgG
α-Gal3
α-Gal3
α-Gal3
α-Gal3
α-Gal3
Input
Beads
IgG
α-Gal3
α-Gal3
α-Gal3
α-Gal3
α-Gal3
Co-IP
rGal3BP
IB
CHI3L1
Gal3
(-)
(+)
TD139

Figure 6. Gal3BP competes with Gal3 for binding with CHI3L1.

(**A**) A binding model of N-terminal Gal3 (magenta Asp3-Pro17 from PDB 6FOF) and CHI3L1 (green surface with red/blue/white shades corresponding to O/N/H atoms from PDB 1HJV_A). (**B**) Detailed view from (A) of the binding mode of Asp3-Asn16 of Gal3 (yellow) and CHI3L1 (green). (**C**) Representative IF images showing co-localization of proteins in TS603 cells. Scale bar, 20 μm. (**D**) Immunoblot (IB) analysis of protein binding complexes using Co-IP with Gal3 antibody in TS603-V5-CHI3L1 cells treated with DMSO or TD139 (10 μM for 24 hours). (**E**) Immunoblot analysis of Gal3 and CHI3L1 protein binding in the mixture of recombinant Gal3 and CHI3L1 (200 ng rGal3 + 200 ng rCHI3L1) by adding different amounts of recombinant Gal3BP (0, 100, 200, 400, 800 ng/sample) with or without TD139 (10 μM for 1 hour).

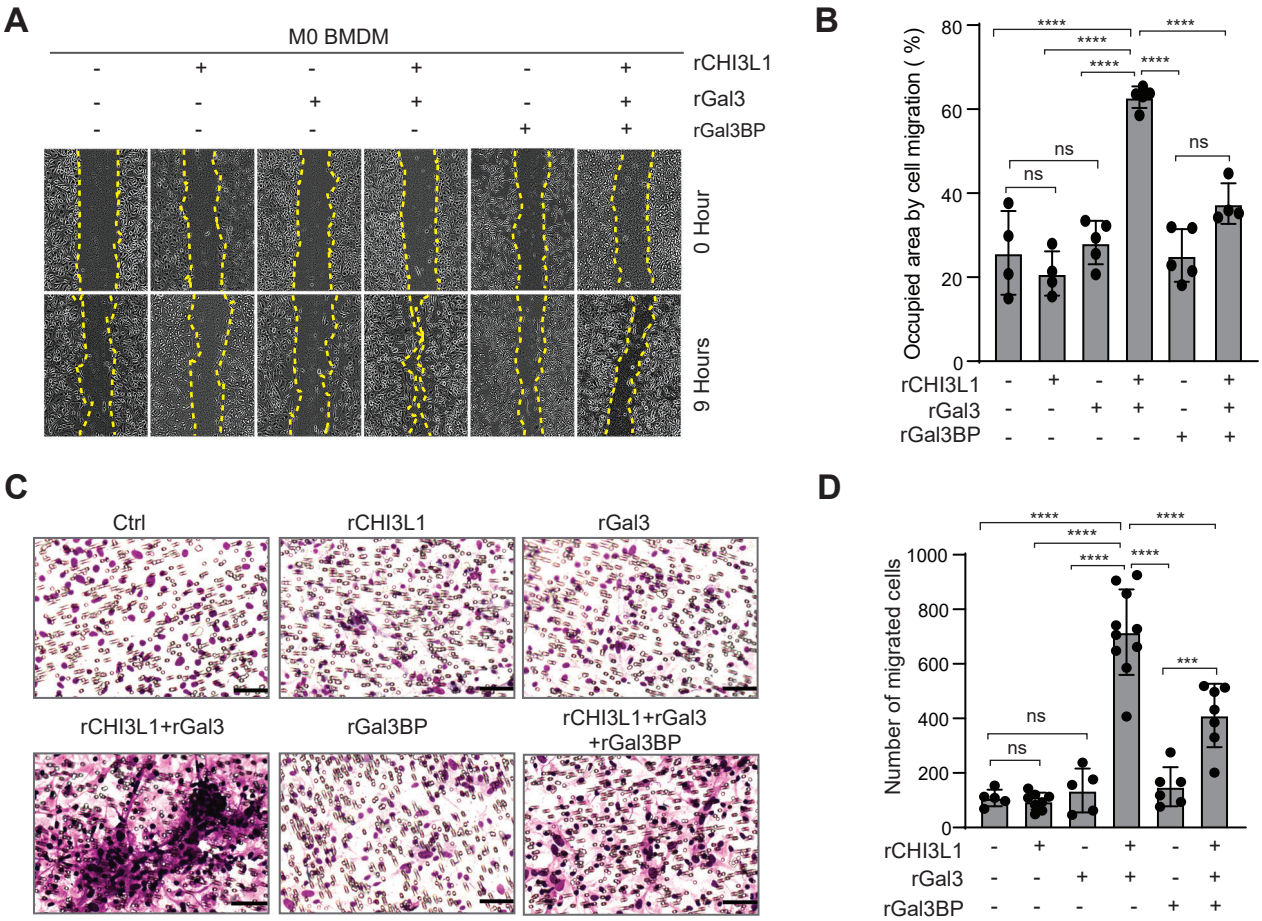
A
M0 BMDM
rCHI3L1
rGal3
rGal3BP
0 Hour
9 Hours
B
Occupied area by cell migration (%)
ns
****
C
Ctrl
rCHI3L1
rGal3
rCHI3L1+rGal3
rGal3BP
rCHI3L1+rGal3
+rGal3BP
D
Number of migrated cells
***
E
M1-like macrophages
P = 0.0329
M2-like macrophages
P = 0.0099
CHI3L1 low and/or LGALS3 low
(n=232)
CHI3L1 high & LGALS3 high
(n=139)

Figure 7. The CHI3L1-Gal3-Gal3BP binding complex regulates BMDM migration.

Representative brightfield images and quantitation for cell migration of M0 BMDMs treated with rCHI3L1 (2.5 μg/mL), rGal3 (2.5 μg/mL), rGal3BP (5.0 μg/mL), and combinations in the scratch-wound healing assay (**A** and **B**) and the Transwell assay (**C** and **D**). Cell migration was assessed by quantifying the occupied area or by counting the number of migrating cells, respectively. Data are presented as the mean ± SD from at least three independent experiments. *P*-value was calculated using one-way ANOVA with Tukey's multiple comparison test; $^{***}P < 0.001$, $^{****}P < 0.0001$; ns represents no significance; scale bar, 50 μm. (**E**) Boxplots showing enrichment of M1/M2-like macrophage signature in two indicated groups of TCGA GBMs. *P*-value was calculated by Wilcoxon rank-sum test.

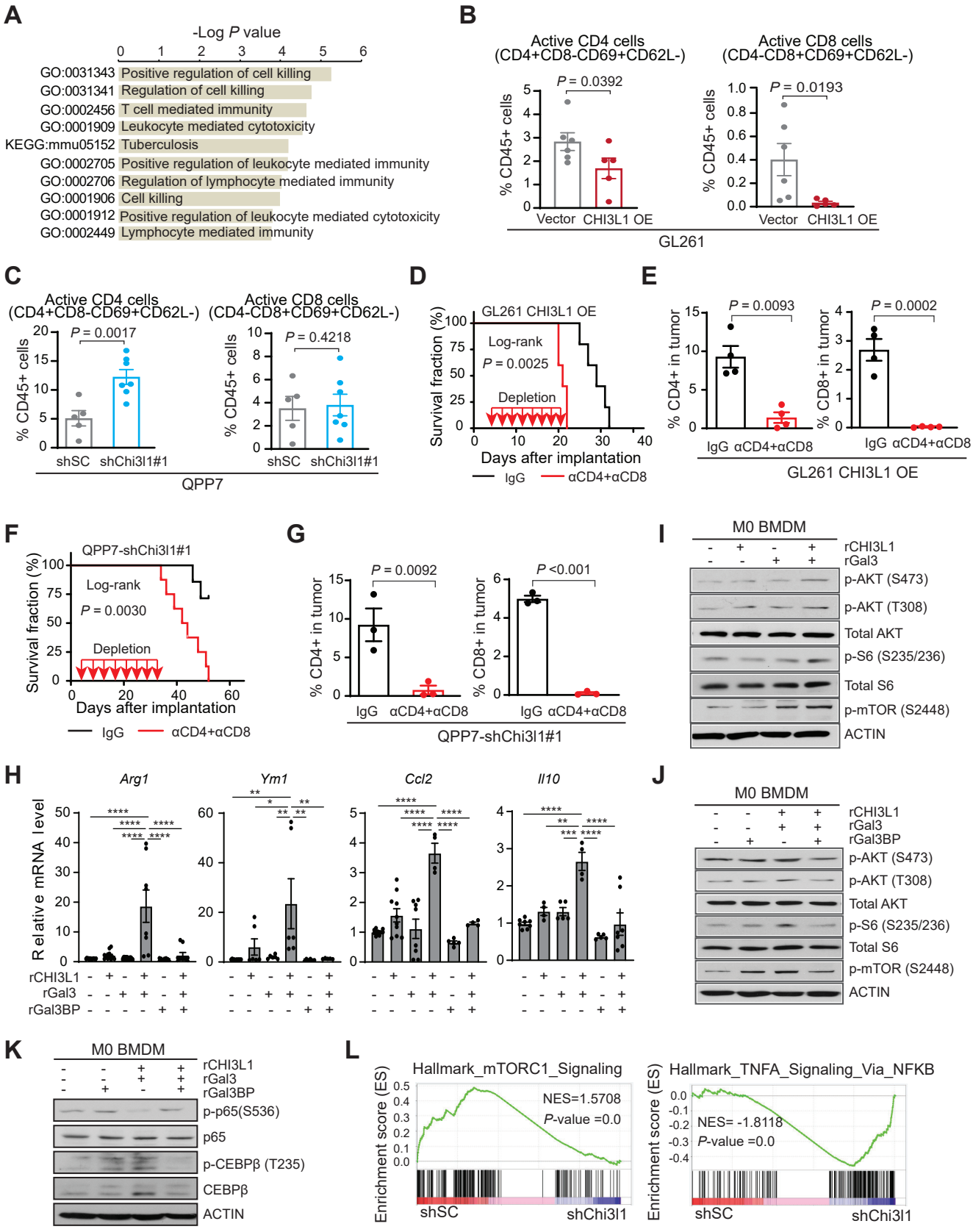
A
-Log P value
0 1 2 3 4 5 6
GO:0031343 Positive regulation of cell killing
GO:0031341 Regulation of cell killing
GO:0002456 T cell mediated immunity
GO:0001909 Leukocyte mediated cytotoxicity
KEGG:mmu05152 Tuberculosis
GO:0002705 Positive regulation of leukocyte mediated immunity
GO:0002706 Regulation of lymphocyte mediated immunity
GO:0001906 Cell killing
GO:0001912 Positive regulation of leukocyte mediated cytotoxicity
GO:0002449 Lymphocyte mediated immunity
B
Active CD4 cells (CD4+CD8-CD69+CD62L-)
Active CD8 cells (CD4-CD8+CD69+CD62L-)
% CD45+ cells
P = 0.0392
P = 0.0193
Vector CHI3L1 OE
GL261
C
Active CD4 cells (CD4+CD8-CD69+CD62L-)
Active CD8 cells (CD4-CD8+CD69+CD62L-)
% CD45+ cells
P = 0.0017
P = 0.4218
shSC shChi3l1#1
QPP7
D
GL261 CHI3L1 OE
Survival fraction (%)
Log-rank
P = 0.0025
Depletion
Days after implantation
IgG αCD4+αCD8
E
% CD4+ in tumor
% CD8+ in tumor
P = 0.0093
P = 0.0002
IgG αCD4+αCD8
GL261 CHI3L1 OE
F
QPP7-shChi3l1#1
Survival fraction (%)
Log-rank
P = 0.0030
Depletion
Days after implantation
IgG αCD4+αCD8
G
% CD4+ in tumor
% CD8+ in tumor
P = 0.0092
P <0.001
IgG αCD4+αCD8
QPP7-shChi3l1#1
I
M0 BMDM
rCHI3L1
rGal3
p-AKT (S473)
p-AKT (T308)
Total AKT
p-S6 (S235/236)
Total S6
p-mTOR (S2448)
ACTIN
H
Arg1
Ym1
Ccl2
Il10
Relative mRNA level
rCHI3L1
rGal3
rGal3BP
J
M0 BMDM
rCHI3L1
rGal3
rGal3BP
p-AKT (S473)
p-AKT (T308)
Total AKT
p-S6 (S235/236)
Total S6
p-mTOR (S2448)
ACTIN
K
M0 BMDM
rCHI3L1
rGal3
rGal3BP
p-p65(S536)
p65
p-CEBPβ (T235)
CEBPβ
ACTIN
L
Hallmark_mTORC1_Signaling
NES=1.5708
P-value =0.0
Enrichment score (ES)
shSC shChi3l1
Hallmark_TNFA_Signaling_Via_NFKB
NES= -1.8118
P-value =0.0
Enrichment score (ES)
shSC shChi3l1

Figure 8. CHI3L1 protein complexes regulate MDM reprogramming in immune suppression and stimulation.

(**A**) Enrichment of top 10 GO biological pathways in TAMs derived from C57BL/6 mice bearing QPP7 with shChi3l1 compared to shSC. (**B**) Flow cytometry analysis showing active CD4 and CD8 cells in GL261 tumors with CHI3L1 overexpression compared to vector controls. (**C**) Flow cytometry analysis showing active CD4 and CD8 cells in QPP7 tumors with *Chi3l1* KD compared to shSC. Depletion antibodies against CD4 and CD8 (10mg/kg) were injected intraperitoneally every 3 days for a total of 8 times after tumor implantation. Kaplan–Meier tumor-free survival analysis of mice bearing GL261 overexpressing CHI3L1 *vs* vector controls (**D**) and mice bearing QPP7 with *Chi3l1* KD *vs* shSC (**F**). Flow cytometry analysis showing $CD4^+$ and $CD8^+$ cell populations within the tumors from GL261 models (**E**) and QPP7 models (**G**) with antibody depletion. Each dot represents 1 mouse; data are presented as the mean ± SEM; *P*-value was calculated using a one-tailed unpaired *t* test. (**H**) qRT-PCR for indicated gene expression in M0 BMDMs treated with rCHI3L1 (2.5 μg/mL), rGal3 (2.5 μg/mL), rGal3BP (5.0 μg/mL), and combinations for 24 hours. Data are presented as the mean ± SEM from at least two independent experiments. *P*-value was calculated using one-way ANOVA with Tukey's multiple comparison test. $^{*}P < 0.05$, $^{**}P < 0.01$ $^{***}P < 0.001$, $^{****}P < 0.0001$. (**I-K)** Immunoblot analysis of indicated protein levels in M0 BMDMs treated with rCHI3L1 (2.5 μg/mL), rGal3 (2.5 μg/mL), rGal3BP (5.0 μg/mL), and combinations for 30 minutes or 4 hours (p-p65 and p65). (**L**) GSEA plots depicting mTOR1 and TNFA-NFKB signaling pathways in TAMs derived from C57BL/6 mice bearing QPP7 with shChi3l1 compared to shSC. NES stands for normalized enrichment score.

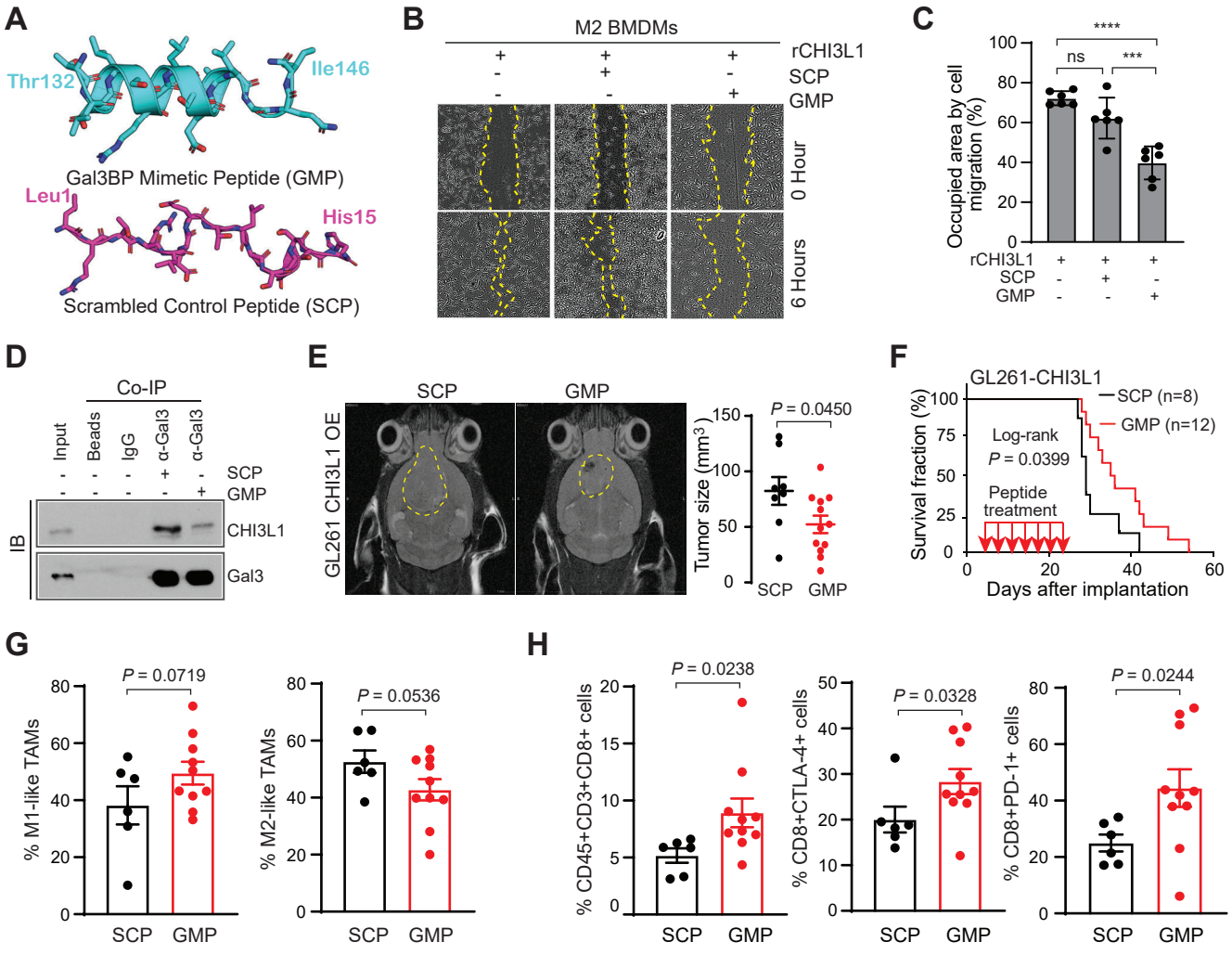
A
Thr132
Ile146
Gal3BP Mimetic Peptide (GMP)
Leu1
His15
Scrambled Control Peptide (SCP)
B
M2 BMDMs
rCHI3L1
SCP
GMP
0 Hour
6 Hours
C
Occupied area by cell migration (%)
ns
***
****
rCHI3L1
SCP
GMP
D
Co-IP
Input
Beads
IgG
α-Gal3
α-Gal3
SCP
GMP
IB
CHI3L1
Gal3
E
SCP
GMP
GL261 CHI3L1 OE
Tumor size (mm3)
P = 0.0450
F
GL261-CHI3L1
SCP (n=8)
GMP (n=12)
Log-rank
P = 0.0399
Peptide
treatment
Survival fraction (%)
Days after implantation
G
% M1-like TAMs
P = 0.0719
% M2-like TAMs
P = 0.0536
H
% CD45+CD3+CD8+ cells
P = 0.0238
% CD8+CTLA-4+ cells
P = 0.0328
% CD8+PD-1+ cells
P = 0.0244

Figure 9. A peptide mimicking Gal3BP attenuates BMDM migration and CHI3L1-induced tumor progression.

(**A**) Snapshot from MD of Gal3BP mimetic peptide (GMP) and scrambled control peptide (SCP). (**B**) Representative brightfield images for cell migration of M2 BMDMs treated with rCHI3L1 (0.6 μg/mL) with/without GMP or SCP at a concentration of 30 μM in the scratch-wound healing assay. (**C**) Cell migration was assessed by quantifying the occupied area of migrated cells. Data are presented as the mean ± SD from at least three independent experiments. *P*-value was calculated using one-way ANOVA with Tukey's multiple comparison test; $^{***}P < 0.001$; $^{****}P < 0.0001$; ns represents no significance. (**D**) Immunoblot analysis of protein binding complexes using Co-IP with Gal3 antibody in THP-1 cells treated with SCP or GMP (20 μM for 24 hours). (**E**) Representative MRI from mice after intracranial injection of GL261-CHI3L1 cells after the treatment of SCP and GMP, respectively. Tumor volume was measured by T2 sequences for infiltrative tumors in the mouse brain (yellow line). (**F**) Kaplan–Meier tumor-free survival analysis of mice bearing GL261-CHI3L1 tumors treating with indicated peptides. Frequency of M1/M2-like MDMs (**G**) and $CD8^+$ T cells with expression of PD-1 and CTLA-4 (**H**) in tumors derived from syngeneic mice bearing GL261-CHI3L1 under the treatment with GMP *vs* SCP. Each dot represents 1 mouse; data are presented as the mean ± SEM; *P*-value was calculated using a one-tailed unpaired *t* test.

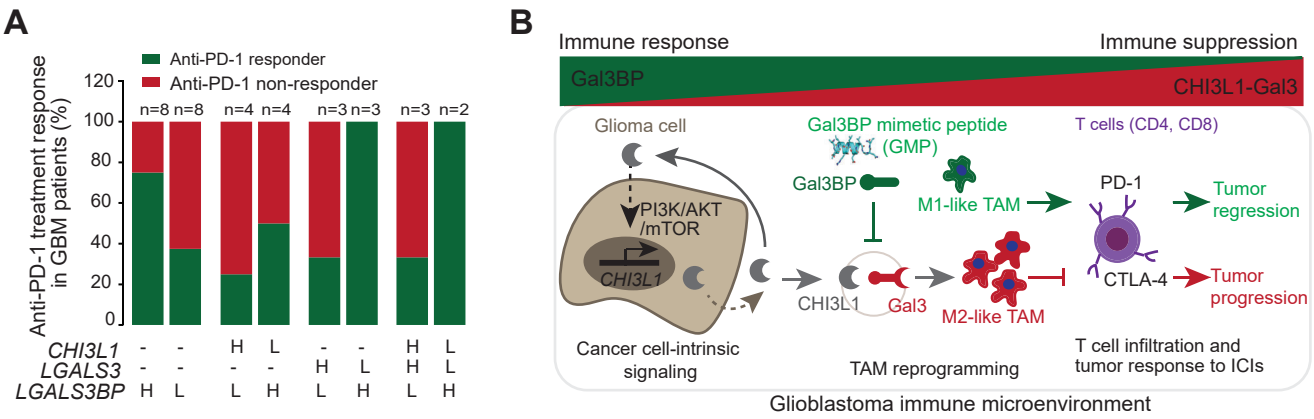
A
Anti-PD-1 responder
Anti-PD-1 non-responder
Anti-PD-1 treatment response in GBM patients (%)
120
100
80
60
40
20
0
n=8 n=8 n=4 n=4 n=3 n=3 n=3 n=2
CHI3L1 - - H L - - H L
LGALS3 - - - - H L H L
LGALS3BP H L L H L H L H
B
Immune response
Immune suppression
Gal3BP
CHI3L1-Gal3
Glioma cell
PI3K/AKT /mTOR
CHI3L1
Cancer cell-intrinsic signaling
Gal3BP mimetic peptide (GMP)
Gal3BP
CHI3L1
Gal3
TAM reprogramming
M1-like TAM
M2-like TAM
T cells (CD4, CD8)
PD-1
CTLA-4
Tumor regression
Tumor progression
T cell infiltration and tumor response to ICIs
Glioblastoma immune microenvironment

Figure 10. The levels of *CHI3L1*, *LGALS3*, and *LGALS3BP* mRNA expression predict anti-PD-1 response in GBM patients.

(**A**) Histogram analysis of the distribution of anti-PD-1 treatment responders and non-responders in GBM patients following anti-PD-1 treatment from a previous dataset (41). The n represents the number of patients characterized with indicted gene expression. (**B**) Schematic cartoon indicates that glioma cell-intrinsic CHI3L1 binding with Gal3 forms a protein binding complex modulating the TAM-mediated immune microenvironment for tumor progression, which is negatively regulated by Gal3BP or Gal3BP mimetic peptide.